2011

Vortex tilting and the enhancement of spanwise flow in flapping wing flight

Spencer Frank
University of Central Florida

VORTEX TILTING AND THE ENHANCEMENT OF SPANWISE FLOW IN FLAPPING WING FLIGHT

by

SPENCER FRANK

A Thesis submitted in partial fulfillment of the requirements
for the Honors in the Major Program
in the Department of Mechanical, Materials, and Aerospace Engineering
in the College of Engineering and Computer Science and
in the Burnett Honors College
at the University of Central Florida
Orlando, Florida

Fall Term 2011

Thesis Chair:
Dr. Seetha Raghavan

ABSTRACT

The leading edge vortex has been identified as the most critical flow structure for producing lift in flapping wing flight. Its stability depends on the transport of the entrained vorticity into the wake via spanwise flow. This study proposes a hypothesis for the generation and enhancement of spanwise flow based on the chordwise vorticity that results from the tilting of the leading edge vortex and trailing edge vortex. We investigate this phenomenon using dynamically scaled robotic model wings. Two different wing shapes, one rectangular and one based on *Drosophila melanogaster* (fruit fly), are submerged in a tank of mineral oil and driven in a flapping motion. Two separate kinematics, one of constant angular velocity and one of sinusoidal angular velocity are implemented. In order to visualize the flow structure, a novel three dimensional particle image velocimetry system is utilized. From the three dimensional information obtained the chordwise vorticity resulting from the vortex tilting is shown using isosurfaces and planar slices in the wake of the wing. It is observed that the largest spanwise flow is located in the area between the chordwise vorticity of the leading edge vortex and the chordwise vorticity of the trailing edge vortex, supporting the hypothesis that the vortex tilting enhances the spanwise flow. Additionally the LEV on the rectangular wing is found to detach at about 80% span as opposed to 60% span for the elliptical wing. Also, two distinct regions of spanwise flow, one at the base and one at the tip, are observed at the beginning of the sinusoidal kinematic, and as the velocity of the wing increases these two regions unionize into one. Lastly, the general distribution of vorticity around each wing is found to be nearly the same, indicating that different wing shapes do not greatly affect the distribution of vorticity nor stability mechanisms in flapping flight. In summary the tilting mechanism helps to explain the overall flow structure and the stability of the leading edge vortex.

DEDICATION

This thesis is dedicated to my family. You have shown me that with support and perseverance one can overcome.

ACKNOWLEDGMENTS

First, I would like to thank my thesis advisor, Dr. Seetha Raghavan. Thank you for constantly challenging me and inspiring me. I would also like to extend a special thanks to my thesis committee Dr. Jayanta Kapat, Dr. Marcel Ilie, and Dr. Xinyan Deng. Additionally the Purdue Bio-Robotics group, Dr. Xinyan Deng, Bo Cheng, and Giovanni Barbera, were very helpful in providing guidance, assistance, and experimental data during my summer at Purdue. I also would like to extend my gratitude to Vicki Leavitt and the 2011 Purdue Summer Undergraduate Research Fellowship (SURF) staff for selecting me to take part in what became the most productive summer of my life (thus far). TSI Inc. for the use of the Volumetric 3-Component Velocimetry (V3V) System which provided high quality data. For giving great feedback in preparation for my thesis defense I would like to thank Dr. Raghavan's entire research group.

I would also like to thank all the staff at the Burnett Honors College, especially Denise Crisafi, for answering any questions regarding the thesis process. Also, Dr. Avelino Gonzalez for teaching me how to perform a literature review and define a research problem. Thank you to the Young Entrepreneur and Scholar/Research and Mentoring Program (YES-RAMP) and the National Science Foundation for providing funding for this research.

A special thanks to David Siljee and Jennifer Pritchard for their support throughout the entire thesis process. Last but not least I would like to extend my gratitude to Rene Diaz for his guidance throughout my undergraduate career.

TABLE OF CONTENTS

LIST OF FIGURES

ABBREVIATIONS

LEV	Leading Edge Vortex
TEV	Trailing Edge Vortex
PIV	Particle Image Velocimetry
V3V	Volumetric 3-Component
MAV	Micro Aerial Vehicle
DPIV	Defocusing Particle Image Velocimetry
Re	Reynolds Number
AR	Aspect Ratio
ν	Kinematic Viscosity
ρ	Density
n	Wing Beat Frequency
Φ	Amplitude
R	Wing Length

CHAPTER 1: INTRODUCTION

1.1 MOTIVATION AND BACKGROUND

Insects exhibit one of the most effective evolutionary means of survival - flight. This ability affords them the necessary skills to be very elusive prey. What makes these animals so elusive to capture is their extremely efficient method of flight, flapping wing flight.

Compared to the traditional modes of flight, such as fixed wing and rotary, flapping flight offers far superior maneuverability, the ability to hover, and elevated lift characteristics. The superior maneuverability and ability to hover comes from the complex kinematics. The increased lift is from the unsteady flow structure. The most important part of the flow structure is the Leading Edge Vortex (LEV). It is Polhamus [1] that first explained how the leading edge vortex creates lift, developing a theory which became known as the Polhamus suction analogy. The enhanced lift of the LEV has been a highly studied topic for decades and its characteristics are well documented, but it is the ability of this flow structure to remain stably attached to the wing that has been the subject of much research by the engineering and scientific community for years. There are two prevailing hypotheses that attempt to explain LEV stability. The first is the attenuating effect on the LEV by the downwash created by the tip vortex [2]. The second and more popular hypothesis is that spanwise flow from the base to the tip of the wing is responsible for draining the vorticity of the LEV into the wake of the wing, and thus limiting its growth and delaying LEV detachment in a phenomenon known as delayed stall[3].

The goal of this work is to explain how the spanwise flow develops based on the vortex tilting and chordwise vorticity of the LEV and trailing edge vortex (TEV). To do this a novel three-dimensional particle image velocimetry (PIV) technique called Volumetric 3-Compoent

Velocimetry (V3V) [4] will be employed to obtain the three-dimensional flow structures of a flapping wing. The wing will be submerged in a tank of mineral oil and flapped at a constant angle of attack under two distinct kinematic motions.

Three-dimensional PIV has only been used in a handful of studies involving flapping wing flight[5, 6] and undoubtedly provides superior information over traditional two-dimensional PIV. The reason for this is the highly three-dimensional nature of the flow involved in flapping wing flight. The ability to capture 3D information allows for a very thorough study of flapping wing flight. The 3D data attained eliminates the need to make simplifying 2D assumptions.

If the development of the spanwise flow can be correlated with vortex tilting it would provide new information about the overall flow structure of flapping wing flight. It would also provide further evidence supporting the hypothesis that the spanwise flow is responsible for stabilizing the leading edge vortex.

A more complete understanding of the aerodynamics of flapping wing flight will facilitate the engineering of micro aerial vehicles (MAV). The possibilities and capabilities of MAVs are endless. One potential use for these devices is for national security purposes. A MAV can be used for surveillance in many types of situations, such as surveying urban areas in dangerous parts of the world. The maneuverability and ability to hover offer distinct advantages over fixed wing and rotary wing devices for these type of surveillance missions.

1.2 FLAPPING FLIGHT VS. CONVENTIONAL FLIGHT

There are many distinct differences between flapping wing flight and conventional flight. Flapping wing flight involves unsteady aerodynamics as opposed to the steady aerodynamics found in helicopters and airplanes.

Figure 1 illustrates common methods of flight. Some familiar machines and animals fall under conventional and unsteady aerodynamics. The main difference between unsteady and steady aerodynamics in the context of our study is the different manner in which the lift is produced[7].

For airplanes, helicopters, and birds (during steady flight stages) conventional aerodynamics are employed. The circulation is bounded around the center of the wing and is created in a manner consistent with common aerodynamic theory[8]. The pressure on the bottom

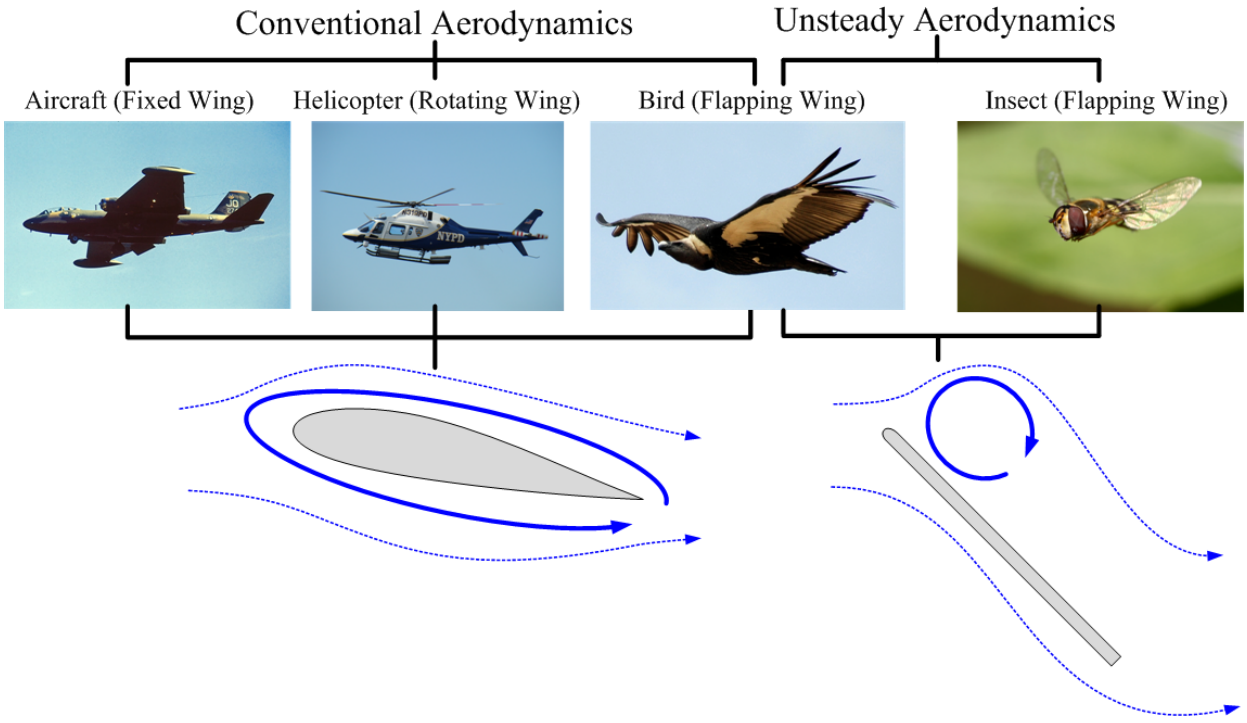

Figure 1: Conventional Aerodynamics vs. Unsteady Aerodynamics

of the wing is higher than the pressure on the top of the wing so the air wishes to move from the bottom to the top, creating lift. Conventional aerodynamics also operate at a very high Reynolds numbers and low angle of attack.

For insects and birds (during transient flight stages) a more complex and less understood method of lift is in place. The circulation is confined to the top of the wing in what is known as a leading edge vortex (LEV). Unsteady flapping wing flight operates at a much lower Reynolds number than fixed wing flight and also incorporates a very high angle of attack compared to conventional flight. This high angle of attack is responsible for the creation of the LEV and will be explained in Section 1.4. The leading edge vortex possesses a very low pressure, and creates a suction force above the wing which is responsible for creating lift. By the nature of flapping wing kinematics the circulation stays attached to the wing in a phenomenon known as delayed stall. In some cases it has been found that 2-5 times more lift can be generated for unsteady aerodynamics compared to conventional.

1.3 KINEMATICS OF FLAPPING WING FLIGHT

The kinematics of insect wing flight can be very complex and varies greatly from species to species and maneuver to maneuver[7]. For example when an insect performs a turning maneuver the kinematics of each wing can be different. For the sake of simplicity many engineers have chosen to use the hovering mode of flapping flight because it provides a consistent and repetitive motion from wing stroke to wing stroke.

The typical wing kinematic for hovering flight involves four primary motions; upstroke, downstroke, pronation and supination[9]. Upstroke is the translational motion from front to back, downstroke is the translational motion from back to front. Supination is the clockwise rotation at the front of the wing stroke and pronation is counterclockwise rotation at back of the wing

stroke. Pronation and supination are responsible for changing the angle of attack to maintain positive lift for the upstroke and downstroke. Each of these phases of kinematic motion is shown in Figure 2.

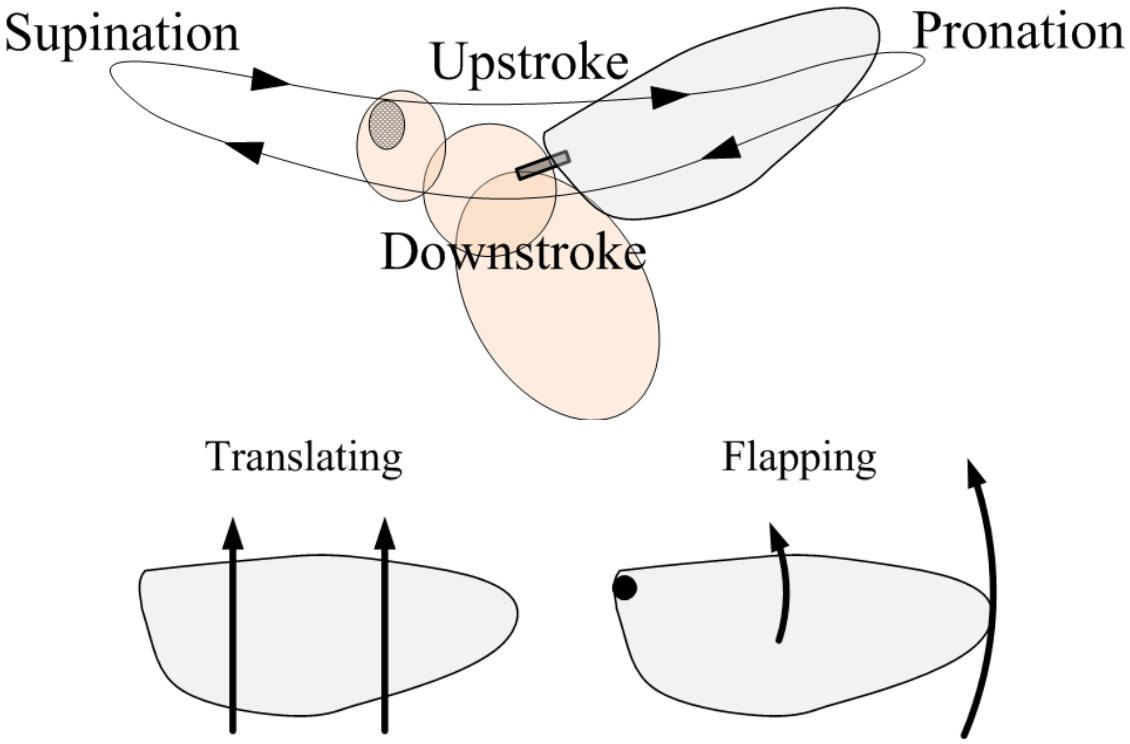

Figure 2: (Top) Phases of insect wing kinematics. (Bottom) Translation vs. Flapping. Adopted from Sane[7].

To differentiate flapping wing flight from translational flight it is important to consider that flapping wing flight involves rotation about a fixed axis, while translational flight involves no rotation. By definition, a two-dimensional wing cannot perform flapping motion[7].

1.4 POLHAMUS SUCTION ANALOGY, DELAYED STALL, AND VORTEX SHEDDING

For a more theoretical explanation of lift in flapping wing flight the Polhamus suction analogy is used frequently[1]. This analogy makes sense of the elevated lift that results from a

LEV. Figure 3 helps to explain the Polhamus suction analogy that was originally developed for high angle of attack delta wings.

For a typical blunt airfoil, the air flows smoothly around the wing. Near the stagnation point at the nose resides a relative low pressure area that results from the flow moving sharply around the wing in this vicinity. The resultant force is parallel and opposite to the flow direction and is small in magnitude. The only lift that is present in this case is the potential lift due to the bound circulation (top of Figure 3)

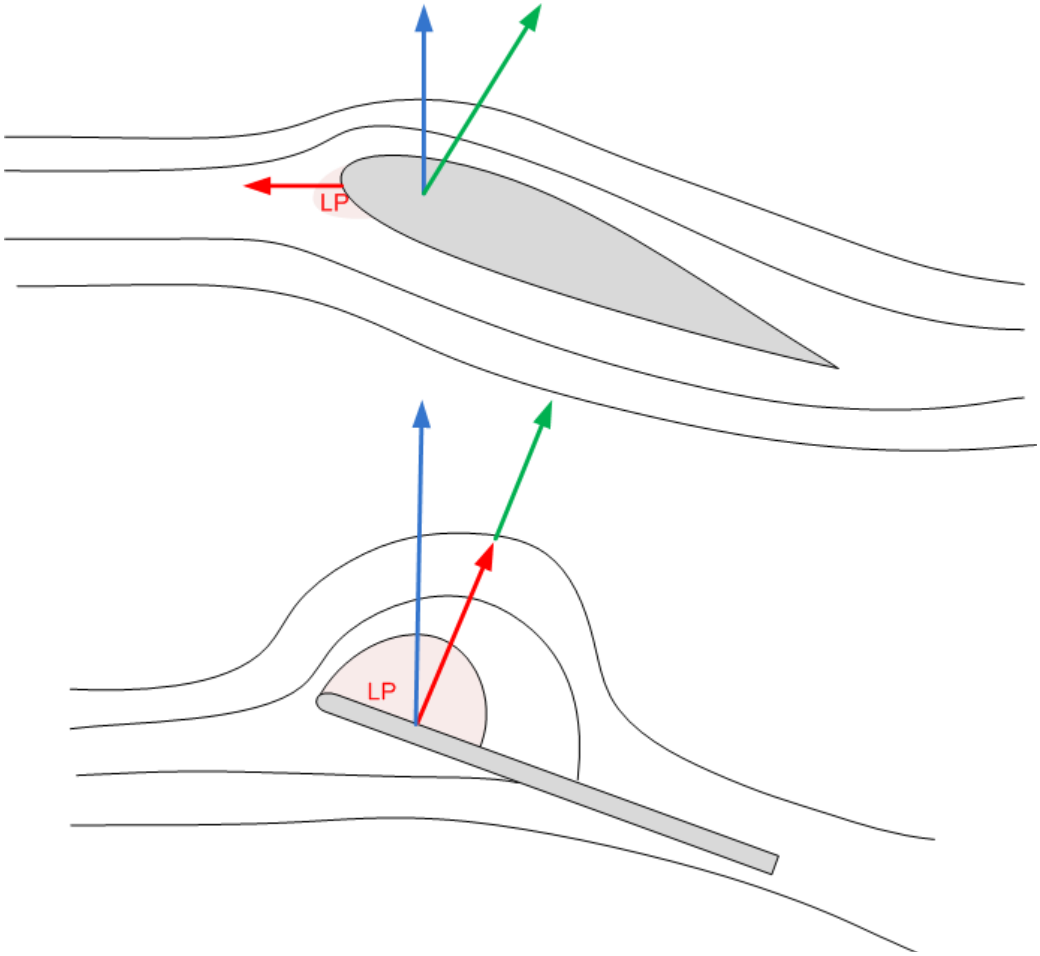

Figure 3: Polhamus suction analogy. For a blunt wing (top) the air moves smoothly around the airfoil and there is a sharp change in flow near the nose of the airfoil, which creates an area of low pressure. For a thin airfoil at high angle of attack (bottom) the flow detaches at the leading edge and reattaches downstream creating an area of low pressure above the wing known as the LEV. This low pressure above the wing is responsible for the elevated lift in flapping wing flight. Adopted from Sane[7].

For flow around a thin airfoil (typical of insect wings, bottom Figure 3) the flow detaches at the leading edge and then reattaches to the airfoil downstream in a phenomenon known as delayed stall. This phenomenon was first visualized by Maxworthy [10]. Because of the detachment near the leading edge an area of very low pressure is present on the top surface of the wing. This low pressure creates a suction force that creates significant additional lift that enhances the overall lift of the wing. This area of low pressure is known as the leading edge vortex (LEV) and has been identified as the most crucial flow structure in flapping wing flight.

Because of the peculiar manner in which lift is created for a thin airfoil at high angle of attack, delayed stall becomes an extremely important concept in insect flight. The principle indicates that as long as the LEV stays attached to the wing, there will be an elevated amount of lift.

To fully understand delayed stall around a thin airfoil it is important to consider the flow in three dimensions. However, before we do this, it is necessary to understand the two dimensional case of the Von Karman Vortex Street.

For the two dimensional case there are alternating low pressure areas aft of the wing. These alternating low pressure areas are associated with the alternating detachment of the LEV and TEV. This phenomenon is known as the Von Karman Vortex Street. Figure 4 illustrates the Von Karman Vortex Street for the two dimensional wing, with the blue representing the negative vorticity generated at the leading edge, and the red representing the positive vorticity generated at the trailing edge. This phenomenon involves a leading edge vortex (blue) and a trailing edge vortex (red) alternately detaching from the body creating high lift during the period which the LEV is attached to the wing. This type of phenomenon occurs frequently for two and three dimensional bodies. After the LEV detaches, the same later occurs for the TEV, and the

alternating sequence continues indefinitely. Some two dimensional studies have shown that the detachment of the LEV for a typical insect wing occurs after two chord lengths of travel[11].

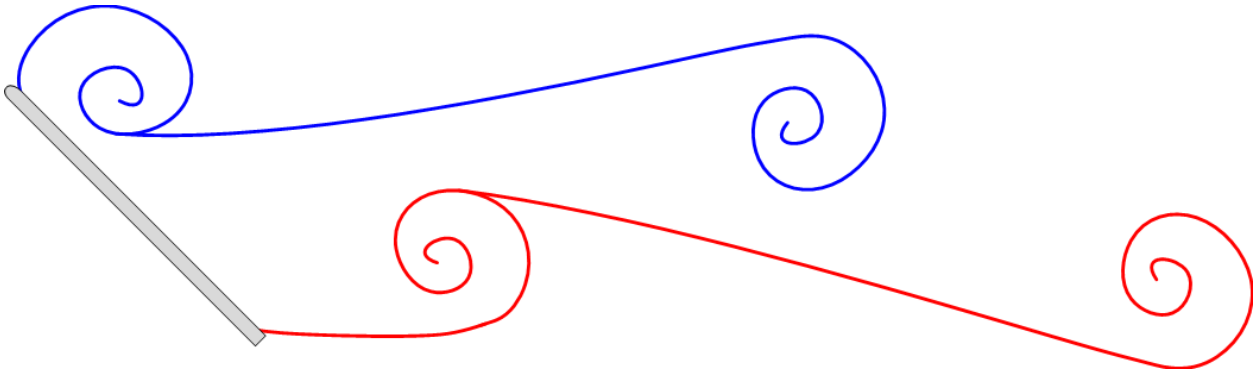

Figure 4: Von Karman Vortex Street for a two dimensional wing

In three dimensions the vortex dynamics are different. The main reason being the flow is no longer constrained to two dimensions, but now has a third dimension that could provide an outlet for the energy that builds up in the LEV as shown in Figure 5. With this ability, the vorticity of the vortex can be transported from the base of the wing to the tip of the wing via spanwise flow. If the vorticity is drained from the vortex at a rate equal to the amount of vorticity that is being generated at the leading edge, then the vortex can attain a stable condition, and it can remain attached to the wing for a prolonged period of time (delayed stall) creating a condition of high lift throughout a wing stroke.

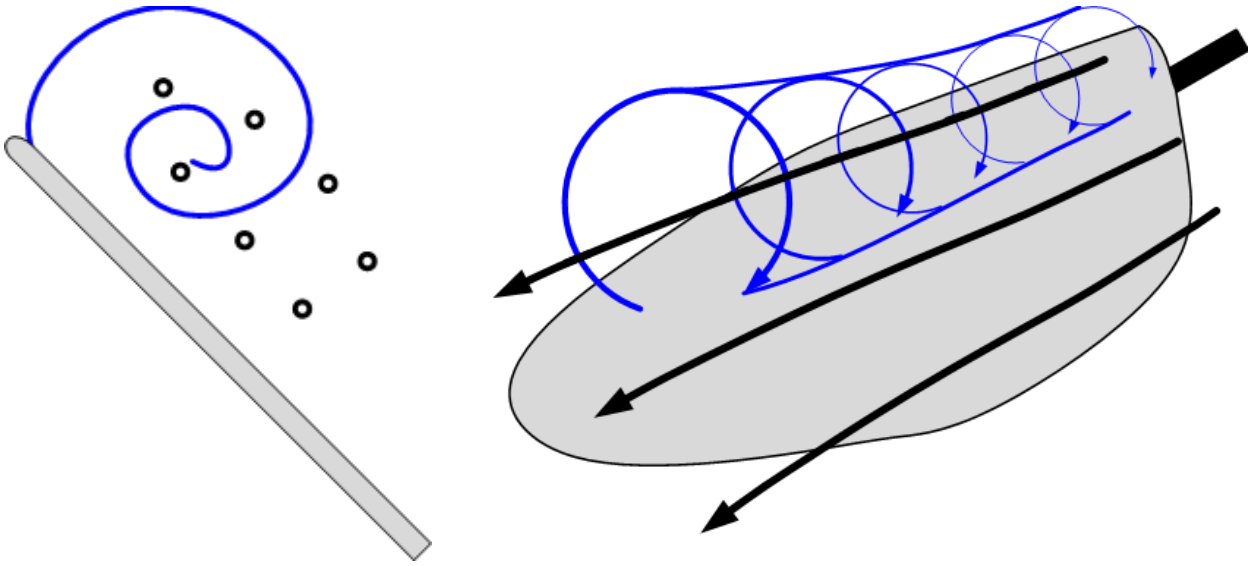

Figure 5: In three dimensions the vorticity entrained in the leading edge vortex can be transported to the tip of the wing via spanwise flow. (Left) Spanwise flow, represented by black dots (out of page). (Right) Black arrows represent the spanwise flow from the base to the tip.

The three dimensional nature of flapping wing flight makes the vortex dynamics fundamentally different from the two dimensional case. The ability of the vorticity to be drained into the wake of the wing in three dimensions is what allows the delayed stall to occur for a prolonged period, thus providing the elevated lift in flapping wing flight.

1.5 THE LEADING EDGE VORTEX AND OVERALL FLOW STRUCTURE

The leading edge vortex has been identified as the most critical flow structure in flapping wing flight because it is responsible for creating lift [2, 3, 12]. Because of its importance it is very highly studied, thus there is a lot of information that explain its formation, location, and strength for various wing shapes and various Reynolds numbers.

To fully understand the leading edge vortex, it is necessary to have an understanding of the entire flow structure of an insect wing. For simplicity sake we will start with a two

dimensional view of the general flow structure and then generalize to the actual three dimensional case.

For the two dimensional case there are two primary flow structures known as the leading edge vortex (LEV) and the trailing edge vortex (TEV) as shown in Figure 6. These vortices are formed in a manner consistent with the Von Karman Vortex Street outlined in the previous section. The leading edge vortex has a clockwise rotation, and the trailing edge vortex has a counterclockwise rotation. Both of these vortices are induced by the vortex shedding that occurs due to the high angle of attack that is typical of flapping wing flight.

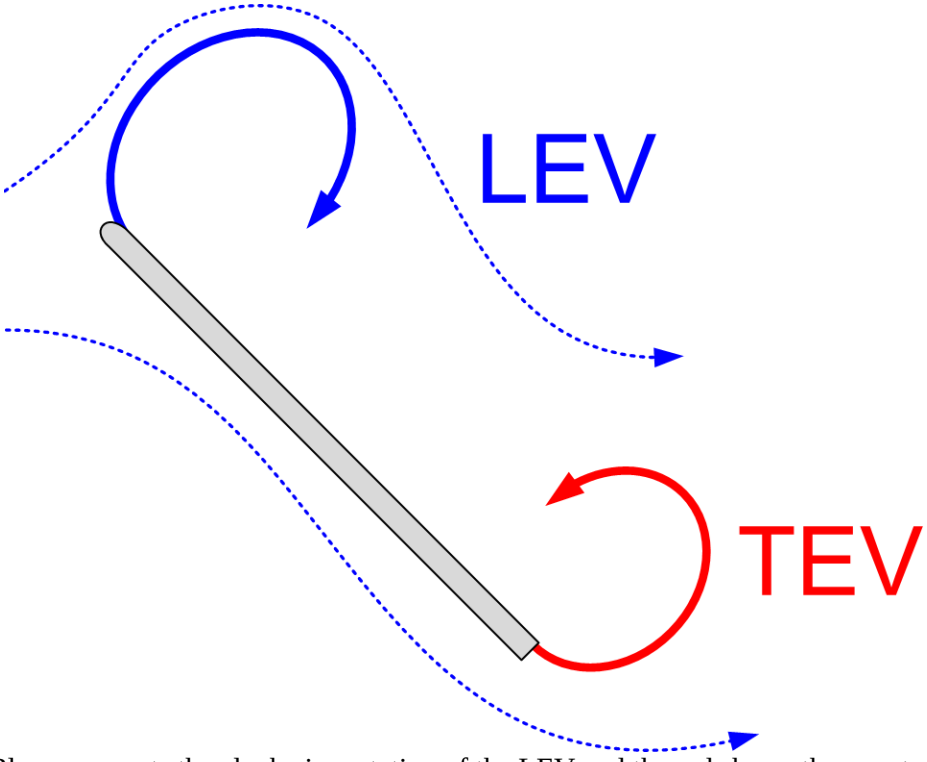

Figure 6: Blue represents the clockwise rotation of the LEV and the red shows the counterclockwise rotation of the TEV.

For more complete visualization a three dimensional schematic, Figure 7 shows the actual path of a typical LEV for a flapping wing. This path of the LEV was first shown by Maxworthy[13]. It is seen that the leading edge vortex follows the leading edge up to about

three-quarters of the span, then detaches. The LEV detachment is due to the increasing strength of the LEV from higher flow velocity as it approaches the tip. Shyy et al. [14] computationally demonstrated that, for Hawkmoths, which operate at Reynolds numbers around 6000, the LEV usually stays attached until about 75% of the span. On the other hand, due to the lower Reynolds number of fruit flies, the LEV of a fruit fly stays attached almost all the way until the tip of the wing.

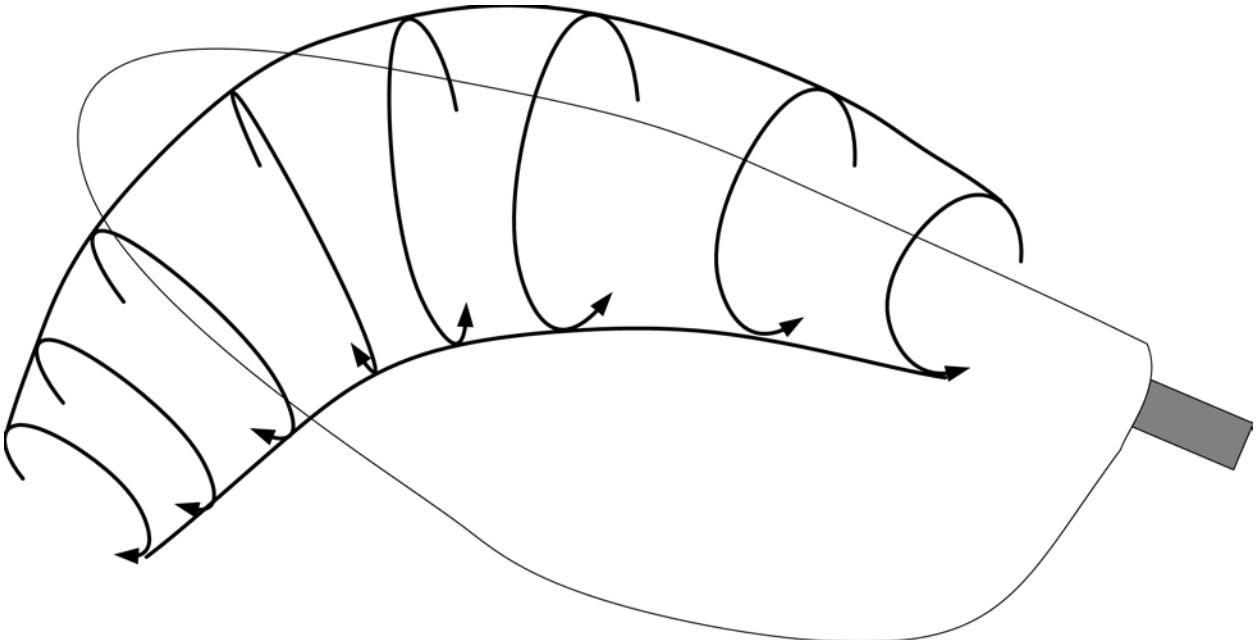

Figure 7: LEV Visualization for a three dimensional wing

Now that the LEV has been clearly introduced, the entire flow structure of a flapping wing can be introduced. Figure 8 shows a complete schematic of a flapping wing flow structure.

Although each flow structure seems independent, they are all interrelated. As the wing is accelerated from rest, a starting vortex (SV) is formed and is immediately shed into the wake. As the wing accelerates, a stable LEV and TEV forms. At the same time, a tip vortex (TV2) similar to that of the wingtip vortex of an airplane forms as the higher pressure at the bottom of the wing moves around to the top of the wing. Next the LEV detaches and turns into the wake as another

tip vortex (TV1). While all these flow structures are forming, downwash and spanwise flow are increasing (green lines) due to pressure differences and vortex tilting (as this study hopes to prove). When the wing eventually attains a steady condition, the starting vortex is no longer part of the flow structure as it is far back in the wake.

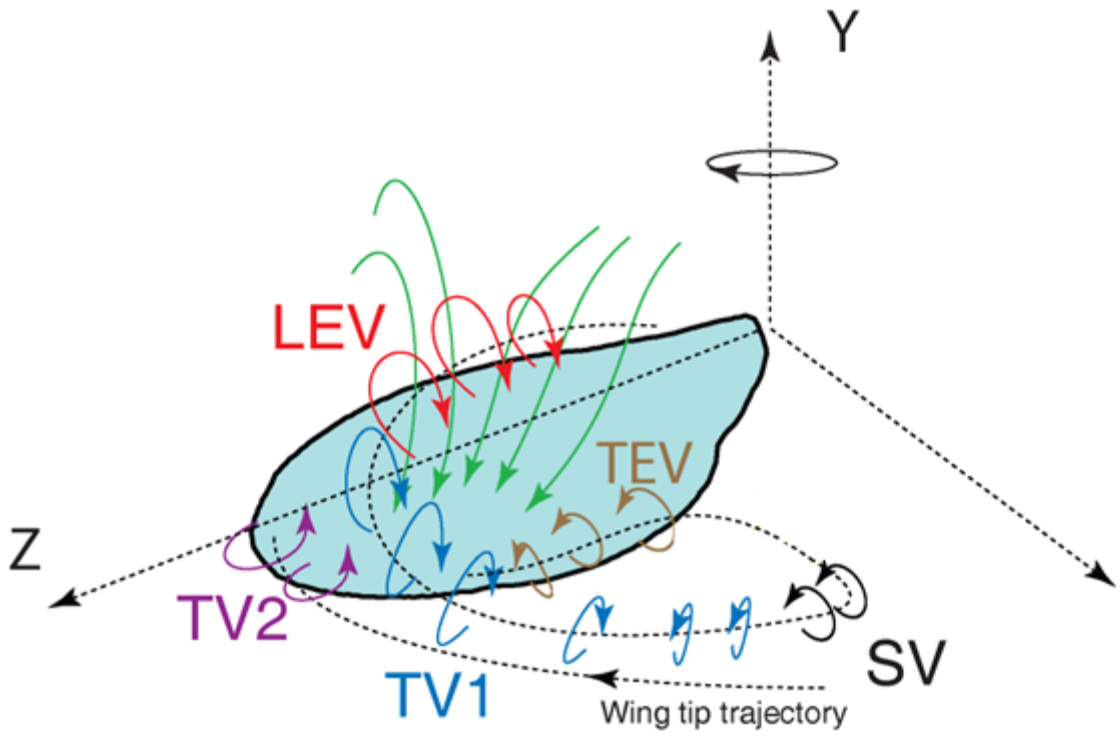

Figure 8: Schematic represents a wing a few moments after it is accelerated from rest. LEV represents the leading edge vortex. TV2 represents the traditional wing tip vortex. TV1 is the tip vortex that is the remainder of the shed LEV. TEV is the trailing edge vortex. SV is the starting vortex.

1.6 VORTEX TILTING AND PROPOSED HYPOTHESIS

Vortex tilting is the mechanism that nominally tilts a vortex so as to give the vortex a small component of vorticity in a direction perpendicular to its core (Figure 9). For flapping wing flight, the predominant component of the LEV and TEV is this spanwise vorticity. The vortex tilting turns some of the spanwise vorticity into chordwise vorticity. From here the term

vortex tilting will be used in conjunction with chordwise vorticity. It is important to note that some of the chordwise vorticity is due to the vortex tilting and some of it is from the tip vortex. In order to differentiate between these two, the chordwise vorticity that results the vortex tilting will be specified.

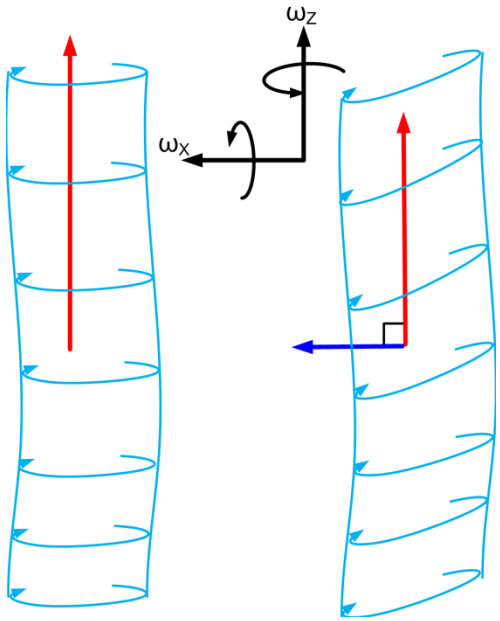

Figure 9: (Left) Non-tilted vortex. Core and vorticity sense are coincident (Red line). (Right) Tilted Vortex. A component of vorticity is perpendicular to the core of the vortex (Blue).

Because vortex tilting does not exist in a two dimensional flow, the ability of the V3V system to accurately capture three-dimensional flow fields provides an opportunity to analyze vortex tilting in a manner not possible before. First, to prelude into vortex tilting analysis by experimentation, it is necessary to first provide a simple theoretical basis for vortex tilting.

First we write the Navier-Stokes equation in terms of vorticity in a rotating frame of motion (Equation 1) [15]. The left hand side of the equation, $D\omega/Dt$, represents the rate of change of vorticity following a fluid particle. The third term on the right of the equation, $\nu\nabla^2\omega$, represents the rate of change of vorticity from molecular diffusion. The second term, $1/\rho^2 *$

$\nabla\rho \times \nabla$p, is a measure of the baroclinicity, the dependence of density on temperature and pressure as opposed to only pressure dependence. The first term on the right, $(\omega + 2\Omega) \cdot \nabla$u, is a measure of vortex tilting, turning, and stretching and it's thus crucial to vortex dynamics in this study. For a clearer description of the first term, we will assume a barotropic, inviscid, and non-rotating frame so that Equation 1 be simplified to Equation 2.

Equation 1

$$\frac{D\omega}{Dt} = (\omega + 2\Omega) \cdot \nabla \mathrm{u} + \frac{1}{\rho^2}\nabla\rho \times \nabla \mathrm{p} + \nu\nabla^2\omega$$

Equation 2

$$\frac{D\omega}{Dt} = (\omega \cdot \nabla)\mathbf{u} = \omega\frac{\partial \boldsymbol{u}}{\partial s}$$

Equation 3 Equation 4 Equation 5

$$\frac{D\omega_s}{Dt} = \omega\frac{\partial u_s}{\partial s} \qquad \frac{D\omega_n}{Dt} = \omega\frac{\partial u_n}{\partial s} \qquad \frac{D\omega_m}{Dt} = \omega\frac{\partial u_m}{\partial s}$$

Stretching Turning Tilting

Using a natural coordinate system with *s* along the vortex line (or core), *n* away from the center of curvature, and *m* along the third normal, the $\omega \cdot \nabla$u term can be broken into three components, vortex stretching, turning, and tilting.

Equation 3 represents the vortex stretching due to velocity u_s along the vortex line, or core. Equation 4 and Equation 5 represent the turning and tilting of the vortex from the velocities u_n and u_m that are normal to the vortex line. Because of the rotational motion of the wing, there

is likely to be a velocity gradient $\partial u_n/\partial s$ and $\partial u_m/\partial s$ along the wing that could induce vortex tilting and turning.

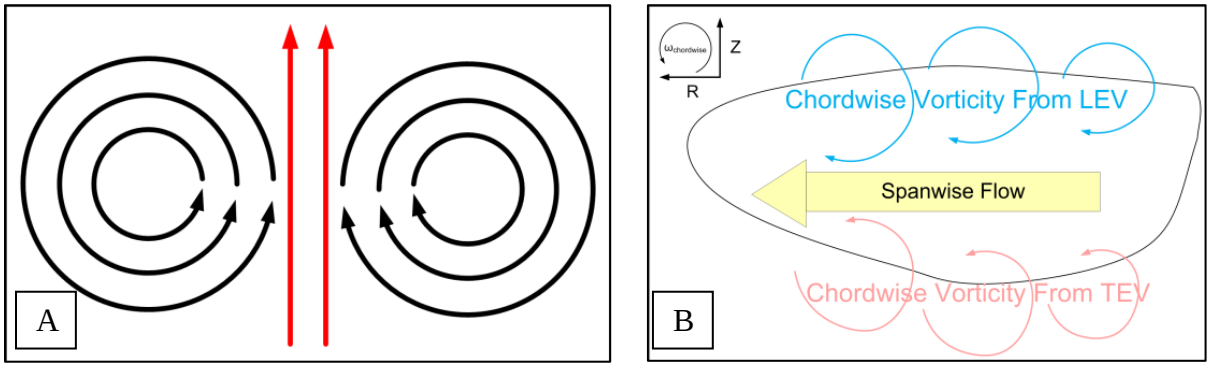

Figure 10: (A) Analogous vortex pair inducing flow between each other
(B) Chordwise vorticity that results from vortex tilting and how it can induce spanwise flow

In our case the vortex tilting would be of the LEV and TEV. This vortex tilting of the LEV and TEV would be analogous to a vortex pair of opposite signs that induces a flow between them, such as seen in Figure 10 (A). Figure 10 (B) shows the proposed hypothesis of how the chordwise vorticity that results from vortex tilting can induce a spanwise flow on a flapping wing. It is this spanwise flow that this study wishes to identify and correlate with the vortex tilting of the LEV and TEV.

It is hypothesized that the chordwise vorticity that results from the vortex tilting of the Leading Edge Vortex and Trailing Edge Vortex can act to significantly enhance the spanwise flow of a flapping wing.

As prior research shows, the spanwise flow in flapping wing flight is responsible for the stability of the LEV. This research aims to show the source of the spanwise flow.

1.7 OVERVIEW

Chapter 2 describes the basic theory relating to the LEV and the state of the art. The experimental methods will be outlined in Chapter 3, with a description of the facility, wing shape and kinematics, measurement methods, and post-processing. In Chapter 4, the constant velocity rectangular wing case will be the basis of the results, and after the rectangular wing has been fully described, the results will be compared to that of the elliptical wing. The sinusoidal case for each wing will then be presented in Chapter 5. Finally, in Chapter 6, the conclusion will summarize the finding that there is a strong correlation between the vortex tilting and spanwise flow for a rotating wing.

CHAPTER 2: THEORY AND BACKGROUND OF LEADING EDGE VORTEX

The most critical and interesting flow structure in insect flight is the leading edge vortex (LEV). This flow structure has been identified as the primary cause of lift in flapping wing flight [2, 3, 12]. The question of significant interest associated with the LEV is how it remains stably attached to the wing, for if it were to detach all lift would be lost, as happens during airplane stall. The difference is that for a flapping wing the LEV does not detach for the duration of the wing stroke in a phenomena known as delayed stall [1, 10]. During delayed stall in flapping wing flight, a large suction force is present above the wing which explains the high lift relative to fixed wing flight. Because of the importance of the stability of the LEV, it is an extensively studied topic, and there are various hypotheses that attempt to explain LEV stability.

The most commonly accepted hypothesis is based on the spanwise flow that develops from base to tip in flapping flight [16-18]. Ellington [3] showed that this spanwise flow exists by releasing blobs of smoke at the base of a flapping wing and observing the movement of the blob. He then went on to explain that this spanwise flow must be responsible for stabilizing the LEV by transporting vorticity from the core of the LEV into the wake.

Other studies have been carried out that propose an alternative hypothesis. Birch and Dickinson [2] carried out an experiment that used edge baffles to block the spanwise flow of a wing as it flapped. When it was observed that the LEV still remained attached, regardless of the spanwise flow, it was proposed that it was not the spanwise flow that stabilized the LEV, but instead, it was the attenuating effect of the downwash from the tip vortex that limited the size of the LEV and kept it attached to the wing. A computational study was also carried out [19] that studied the tip vortices that resulted from two different wing motions by Shyy et. al. [19]. Shyy

determined that the tip vortices served to anchor the rotational starting vortex, thus helping to anchor the LEV and supporting the claims made by Birch and Dickinson.

Efforts have also been made to reconcile these two competing trains of thought. Birch [18] carried out a two-dimensional Particle Image Velocimetry (PIV) study to measure the spanwise flow of a flapping wing at Reynolds numbers 120 and 1400. It was found that at the higher Reynolds number an intense spanwise flow was present within the vortex core, and the spanwise flow was absent at the lower Reynolds number. In both cases the LEV remained attached. This suggests that the mechanism responsible for the stability of the LEV takes different forms at different Reynolds numbers. Other computational studies by Shyy [14] also supports this claim, however, more recent studies suggest that stability does not depend on Reynolds number [17].

Lentink and Dickinson postulated that the centripetal and Coriolis acceleration inherent in rotating motion is responsible for the stability of the LEV, and that stability does not depend on Reynolds number [17, 20]. The stability of the LEV was also determined to be dependent on certain shape parameters of the wing such as the Rossby number. These findings also support the hypothesis that spanwise flow was responsible for LEV stability.

Some research has also been aimed at the role of the tip vortex in flapping wings. Ringuette [21] found that the tip vortex contributes substantially to the overall plate force and that the interaction between the tip vortex and LEV generates a high transient drag peak. Trizila [22] modeled the forces around a flat-plate for different kinematic motions and determined that, depending on the conditions, the tip vortex could either help or degrade the aerodynamics of a three-dimensional plate. Birch and Dickenson [2] also considered the tip vortex to be instrumental in the stability of the LEV, and claimed that it anchored the LEV to the wing.

Additionally, some theoretical models have been developed to account for the tip loss in flapping wing flight [23, 24]. All of these different ideas about the role of the tip vortex led to its nominal consideration in this study.

New methods for flow visualization and quantification have been employed recently and offer a great opportunity to study three-dimensional flow structures in insect flight [5, 6, 25-27]. This new method called Volumetric Three-Component (V3V) PIV is provided by TSI Inc. [4] and offers higher fidelity results than other three-dimensional flow measurement methods such as stereoscopic PIV [28-30]. Kim and Gharib [5, 25] used 3D Defocusing Digital Particle Image Velocimetry (DPIV) to visualize and quantify the flow structure dynamics of a flapping wing. It was found that vortex tilting, the tilting of vorticity in a direction normal to its core, induces a spanwise flow for a rotating rectangular wing which may stabilize the LEV. Because vortex tilting is non-existent in two-dimensional flows, the ability to use three dimensional PIV offers new opportunities for studying the overall flow structure of a flapping wing and the effects of vortex tilting on LEV stability. The high fidelity of the measurements by Kim and Gharib [25] prompted the further study of the effects of vortex tilting on spanwise flow through the use of three-dimensional PIV.

The wing kinematics and wing shapes chosen for this study were chosen for their wide use in many studies to date. This facilitates easy comparison for the results obtained from this study. The rectangular wing chosen is convenient for comparison to the results found in various studies [5, 19, 21, 28, 31-36]. Additionally the fruit-fly wing (elliptical case) has been highly studied in many experiments [37-39] which once again provides easy comparison to independently obtained results. The Reynolds number for this study was chosen based on

information provided by Shyy's review paper [40]. The wing kinematics are based on Kim and Gharib [5] for their simplicity.

CHAPTER 3: EXPERIMENTAL METHODS

In this study, dynamically scaled robotic wings are rotated at constant angle of attack in oil at 1) a constant angular velocity and 2) a sinusoidal angular velocity. The V3V system is used to obtain the three-dimensional flow structure. Two different wing shapes are used, one rectangular, and one an elliptical wing modeled on *Drosophila melanogaster* (fruit fly). By obtaining the three dimensional flow structure, the tilted components of the LEV and TEV are identified. Special attention is paid to the position and magnitude of the vortex tilting with respect to the spanwise flow. It is hypothesized that the chordwise vorticity that results from the vortex tilting of the LEV and TEV can act to significantly enhance the spanwise flow of a rotating wing. Because of the importance of the spanwise flow in keeping the LEV stably attached to the wing, the mechanism that creates spanwise flow is very important to insect flight.

3.1 FACILITY

The acrylic tank used for the experiments was 10ft by 2ft by 2 ft and filled with mineral oil. The mineral oil had a viscosity of 9 cSt and a density of 850 kg/m^3. The mechanism used to mount the wing was partially submerged in the center of the tank and far enough away from the walls that the wall effects can be neglected. This mechanism only utilized one servo to create the rotational motion since the angle of attack was fixed. The mechanism used to mount the wing was made of aluminum and submerged approx 4 inches below the water surface. Figure 11 (A,B) shows the facility and experimental setup.

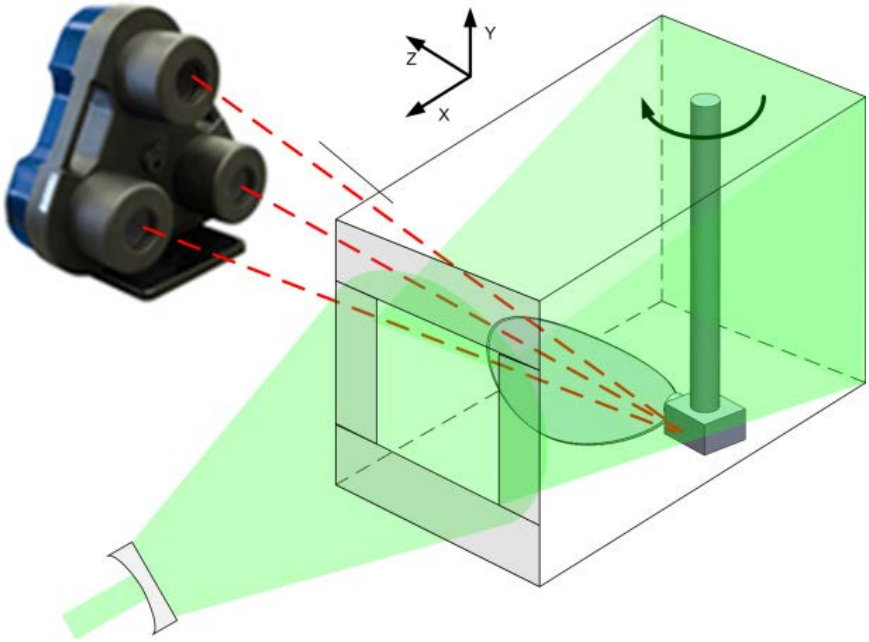

Figure 11: Drawing of experimental setup with V3V System showing probe volume and tape

3.2 WING SHAPE AND KINEMATICS

For this experiment, two wing shapes were used for comparison purposes. The first wing shape was a rectangular wing, and the second was an elliptical wing based on *Drosophila melanogaster* (fruit fly). The dimensions of the rectangular wing was 8 cm span by 2.5 cm chord. The elliptical wing had a span of 7.5 cm and a mean chord length of 2.3 cm. Both wings had an aspect ratio of about 6.5:1. Both wings were made from an acrylic sheet of 0.3 mm thickness. Because of the negligible deformation of the wings, both can be assumed to be rigid [41]. Each of these wings are driven at a constant angle of attack of 45 degrees. Because of the length of the mechanism used to mount the wing to the rotating shaft, the total length from the center of rotation to the wing tip was 12 cm for the rectangular wing, and 11.5 cm for the elliptical wing. An image of the elliptical wing and mounting mechanism is shown in Figure 12 and Figure 13.

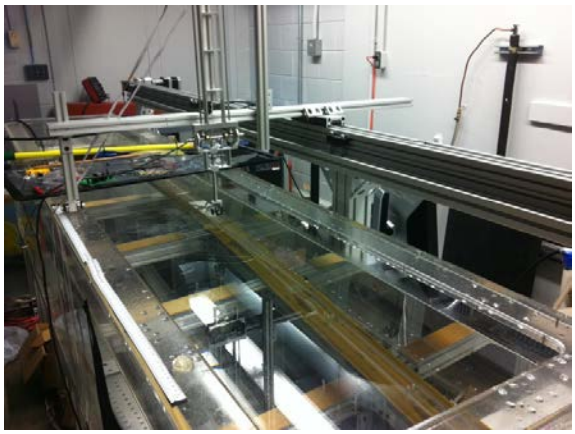

Figure 12 : Picture of tow tank and rotating mechanism

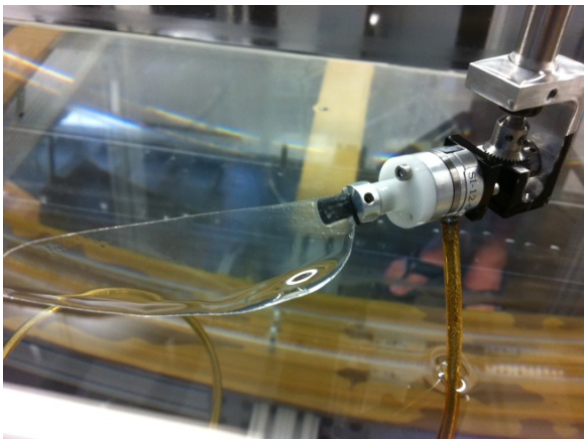

Figure 13 : Elliptical wing and mounting mechanism.

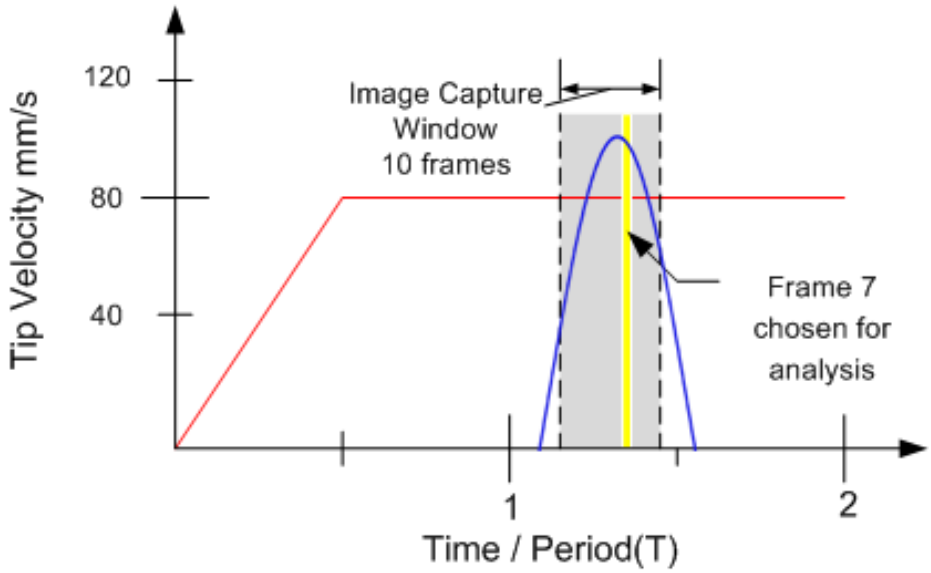

Figure 14: (Red) Kinematics for constant angular velocity motion. Frame 7 used for this kinematic. (Blue) Kinematics for sinusoidal Angular Velocity motion. Frames 3-7 chosen for this analysis.

The kinematics for this study were chosen to 1) provide a constant angular velocity for steady flow analysis and 2) a sinusoidal velocity profile to more accurately model the kinematics of an actual insect. The wing was started from rest and rotated in one complete turn to achieve

its steady angular velocity of 1 rad/s (80mm/s). During its second turn the measurements were taken. For the sinusoidal velocity the wing was accelerated up to a maximum tip velocity of 100 mm/s with a 180 degree total displacement. A description of the kinematics can be seen in Figure 14.

The Reynolds number for this experiment was defined based on a the definition of Reynolds number for a flapping wing (Equation 6) where n is wing beat frequency, Φ is amplitude, R is wing length, AR is aspect ratio, and ν is kinematic viscosity. The calculated Reynolds number of 250 is representative of the fruit fly which operates at Reynolds numbers around 150 to 250.

Equation 6

$$Re = \frac{4\Phi R^2 n}{\upsilon(AR)} = \frac{4\pi R^2 n}{\upsilon(AR)} = 250$$

3.3 MEASUREMENT TECHNIQUES

Using the V3V system (TSI Inc.), a novel three-dimensional flow visualization technique [27], it was possible to reconstruct the full flow field around a rotating wing. Air bubbles were used as seeding, and three pairs of sequential images (Δt = 180us) were taken simultaneously by three four megapixel digital cameras synchronized with an Nd:YAG pulse laser illuminating the air bubbles inside the probe volume. The size of the camera probe volume (14x14x10cm^3), Figure 11, allowed the wing to remain inside the camera view (from 0.3 to 1.4 of the total span length) for a 100° rotation; the axis of rotation was positioned about 3 centimeters beyond the back plane of the volume to avoid undesired laser reflection on the shaft and gearbox. A plano-convave lens was use to make the laser cone that would illuminate the probe volume.

A phase locked loop based on the angular position of the motor was used to synchronize the PIV data with the wing kinematics, capturing one frame each 10° of rotation, for a total of 10 frames throughout the entire rotation. In order to reduce the noise level of the resulting velocity field, each frame was calculated by *ensemble* averaging 10 different images of the wing at the same position and velocity. This allowed for the use of a more sparse particle distribution, with a consequent reduction of the errors related to a higher concentration, e.g. multiple particle identification and obstruction of the particles farther back in the probe volume. Although this technique (as opposed to the instantaneous PIV), does not allow for the capture of unsteady phenomena in the flow field, it greatly reduces noise and uncertainties in the computed velocity field, while still capturing the main features of the flow relevant for the present study. Tape was also used to block out any unnecessary illumination that would introduce noise as seen in Figure 11.

Insight V3V software provided by TSI Inc. was used for particle detection, particle tracking, and velocity field interpolation. The software interpolated all the randomly distributed velocity vectors obtained from the particle tracking algorithm into a convenient 45x45x31 mesh grid ($\Delta x = \Delta y = \Delta z = 3.15$mm) for the three components of velocity at each frame.

Although there were a total of 10 frames captured, one at each wing position, only one frame was needed for the purposes of this study. Because the angular velocity was constant, the only stipulation in selecting which frame to use was whether the entire flow structure would be included or not. It was decided that the seventh frame would be used, because at this wing position, the entire flow structure was included in the probe volume. The position of this frame can be seen in Figure 16.

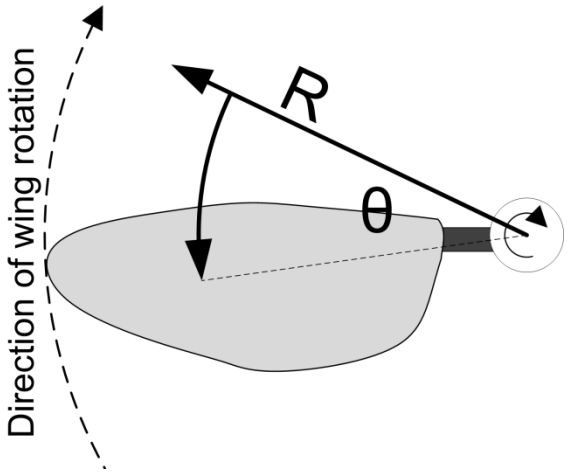

Figure 15: Cylindrical coordinate system. Z is pointing out of the page.

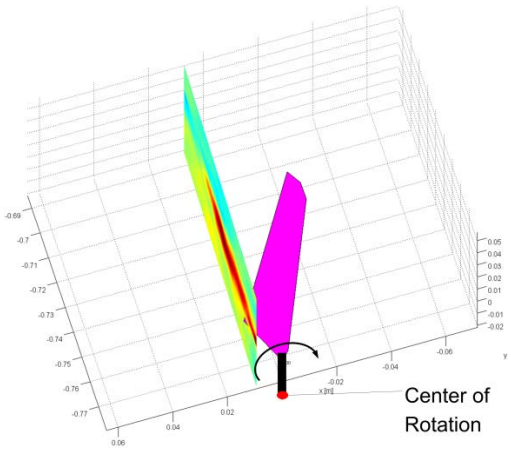

Figure 16: Planar slice taken 25^0 behind leading edge of wing.

3.4 POST PROCESSING AND ANALYSIS

For post processing of the volumetric velocity field data MATLAB was used. For convenience, the Cartesian mesh grid that was output from the Insight V3V software was converted to a cylindrical coordinate system with the origin at the center of rotation. This is a non-rotating reference frame and plots the flow field independent of the wing position. For example, when plotting the flow in the radial direction, all the radial flow radiating out from the origin is plotted and not just the flow that is in the direction of the wing. The coordinate transformation made the data processing and flow visualization easier because of the rotation of the wing and wake structure. Figure 15 shows the cylindrical coordinate system chosen.

In order to determine the actual wing position at each frame the raw images from the three cameras were analyzed. By tracking marked points along the edge of the wing (four for the rectangular wing, six for the elliptical wing) and by estimating their spatial location using the

same camera calibration from the particle identification process, the wing location was determined.

By interpolating between grid points, a surface representing points of constant value, or isosurface, was passed through the flow field to represent the shape of the flow structures. Planar slices were also taken to show the variation in the chosen parameters. These slices were taken chordwise and passed through the center of rotation approximately 25° behind the leading edge for the constant angular velocity case, and 6 mm behind the leading edge for the sinusoidal case. Spanwise velocity and chordwise vorticity were plotted on these planar slices. Refer to Figure 16 for a description of the planar slices taken.

For vorticity visualization, an additive color mapping technique was used to color an isosurface of vorticity magnitude. Figure 17 and Figure 18 show this color mapping technique, with the legend in the corner. For this color mapping the three components of interest, negative spanwise (LEV), positive spanwise (TEV), and negative chordwise (tip vortex and the component of vortex tilting), are represented by blue, red and green respectively. This technique offers clear visualization of the different components of vorticity, as well as showing the regions that are a mix of two components, represented by cyan and yellow. The magenta and white are not used because there can never be a union of positive and negative spanwise vorticity. All of the other components (z vorticity and positive chordwise) are represented by black coloring, since we are limited to three main colors for this visualization technique.

Last, by plotting upwash (Z+) and downwash (Z-) isosurfaces, we were able to get an estimated path of the LEV by using the assumption that on one side of the vortex core the velocity will be roughly opposite of the same point on the opposite side of the core.

CHAPTER 4: CONSTANT ANGULAR VELOCITY TEST CASE

The goal for the constant angular velocity case is to show the correlation between the chordwise vorticity and the spanwise flow for a steady-state condition in which the flow is fully developed around the wing. The flow will be visualized using several methods. These different methods of visualization will give a more complete picture of the flow around the wing.

The first method of visualization is known as tri-color visualization and gives a multi-colored isosurface using a constant vorticity magnitude. This will give an overall visualization of the general flow structure and offers an opportunity to see the distribution of the vorticity as well as the different signs and components of it, all in the same plot. This method will be shown in section 4.1.

The second method of visualization is using isosurfaces to plot different parameters of interest. Chordwise vorticity and spanwise flow will be plotted separately at first to show the overall distribution of each parameter. Next they will be plotted together to show their locations with respect to each other which is convenient in drawing conclusions about the inducement of spanwise flow by chordwise vorticity.

Finally for very clear visualization two-dimensional planar slices are taken in the wake of the wing to show the magnitude variation of chordwise vorticity and spanwise flow. These planar slices allow for the visualization of chordwise vorticity and spanwise flow side by side so conclusions can be drawn about the correlation of their locations with respect to each parameter.

After all the visualization has been carried out a comparison of the wings will be made with respect to their chordwise vorticity and spanwise flow.

4.1 GENERAL FLOW STRUCTURE VISUALIZATION

In order to provide a general description of the flow structure of the rotating wing, an isosurface of vorticity magnitude was used in conjunction with tricolor mapping as described in section 2.4. This visualization technique is similar to the color mapping used by Poelma et al. [30]. Figure 17 shows a tricolor plot of vorticity magnitude. This method is not only useful for visualizing the entire flow structure, but also is useful in showing the distribution of the different components of vorticity.

For the rectangular wing, shown in Figure 17 (A), the LEV (blue) grows very clearly from base to tip, shown by the increasing size. Kim and Gharib [5] found a similar trend for their V3V results with a rotating rectangular wing. Additionally the trailing edge vortex (TEV) is present here (red), and like the LEV it also increases from base to tip. This size increase from base to tip for the LEV and TEV is due to the velocity gradient from the rotational motion. The lower velocity near the wing base generates a smaller LEV and TEV than near mid-span where the velocity and strength of the LEV is much greater. The tip vortex is also a very prominent feature of the flow structure and shows up in light green and cyan which represents chordwise vorticity and a chordwise/spanwise mix respectively. Because of the high angle of attack, there is also a large ω_z component at the tip vortex which can be seen in black. The tip vortex follows the path that is swept out by the wing tip and is created from the sharp edge of the wing in a manner similar to a tip vortex for fixed wing aircraft. There is also an element of spanwise vorticity (dark blue) in the tip vortex. This component comes from LEV after is detaches from the wing and merges with the tip vortex.

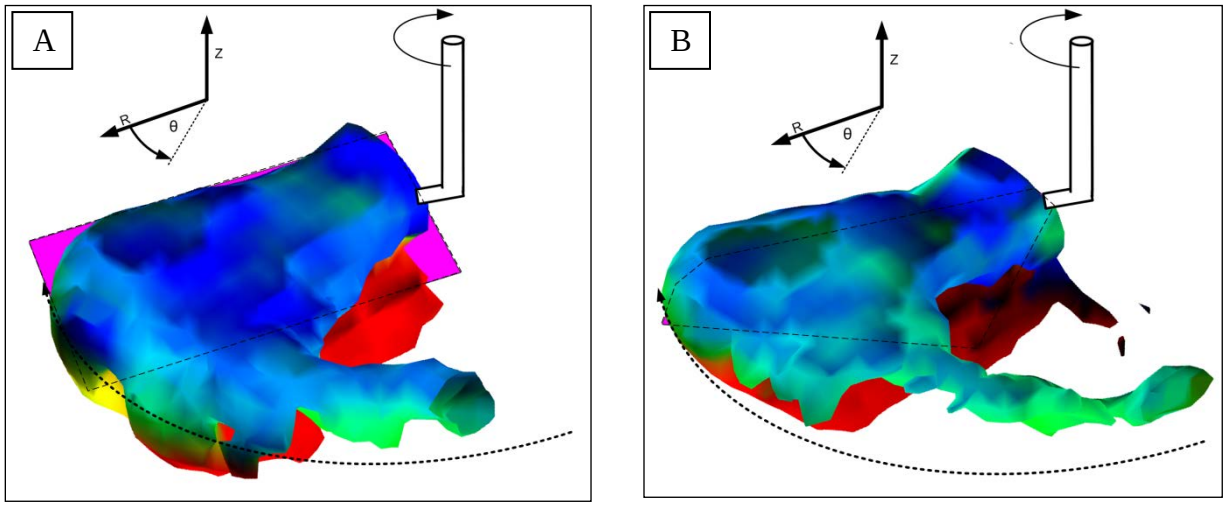

Figure 17: Tricolor plot of vorticity magnitude. ω=3.8 1/s.

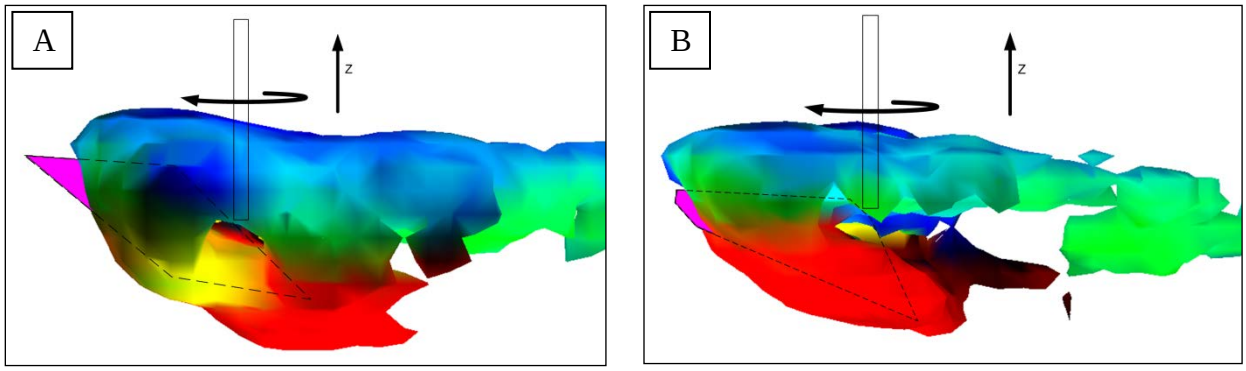

Figure 18: Tricolor plot looking from tip to base. (A) Rectangular (B) Elliptical

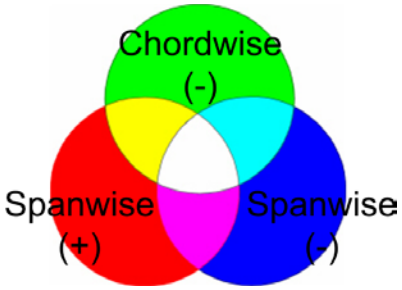

Figure 19: Blue represents negative spanwise vorticity (LEV). Red represents positive spanwise vorticity (TEV). Green shows chordwise vorticity. Yellow and cyan are a mix of components.

The side view found in Figure 18 also demonstrates another interesting feature. A void of vorticity between the LEV and TEV can be seen. As will be explained in a later section, this is the primary area where the spanwise flow is found.

4.2 IDENTIFICATION OF VORTEX TILTING AND SPANWISE FLOW

From Figure 17, it can be seen that the LEV is made up of spanwise vorticity and chordwise vorticity. Because our study aims to determine the effect of vortex tilting on spanwise flow, we need to plot the chordwise vorticity that results from the vortex tilting. To do this isosurfaces showing chordwise vorticity are shown in Figure 20. The yellow isosurface shows the negative chordwise vorticity (LEV) and the cyan isosurface shows the positive chordwise vorticity (TEV). These isosurfaces clearly show the chordwise vorticity distribution around the wing and in the wing wake.

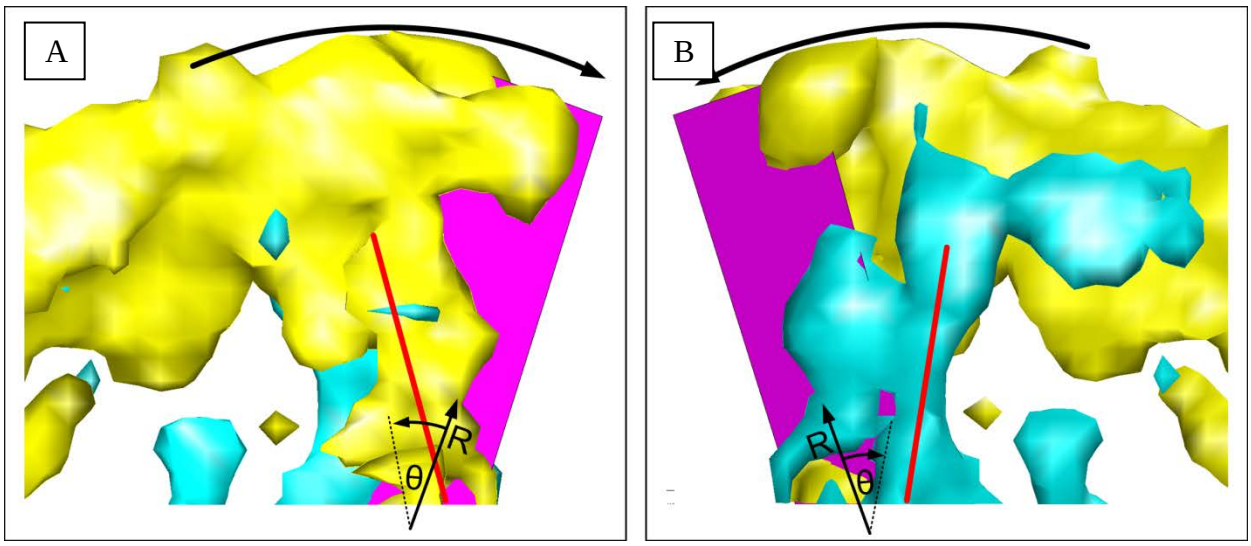

Figure 20: Rectangular Wing. (A) is chordwise vorticity from top of wing. (B) is chordwise vorticity from bottom of wing. Yellow isosurface is ω = - 1.75 1/s. Cyan isosurface is ω=1.3 1/s. Dark black line at wing tip shows direction of wing rotation

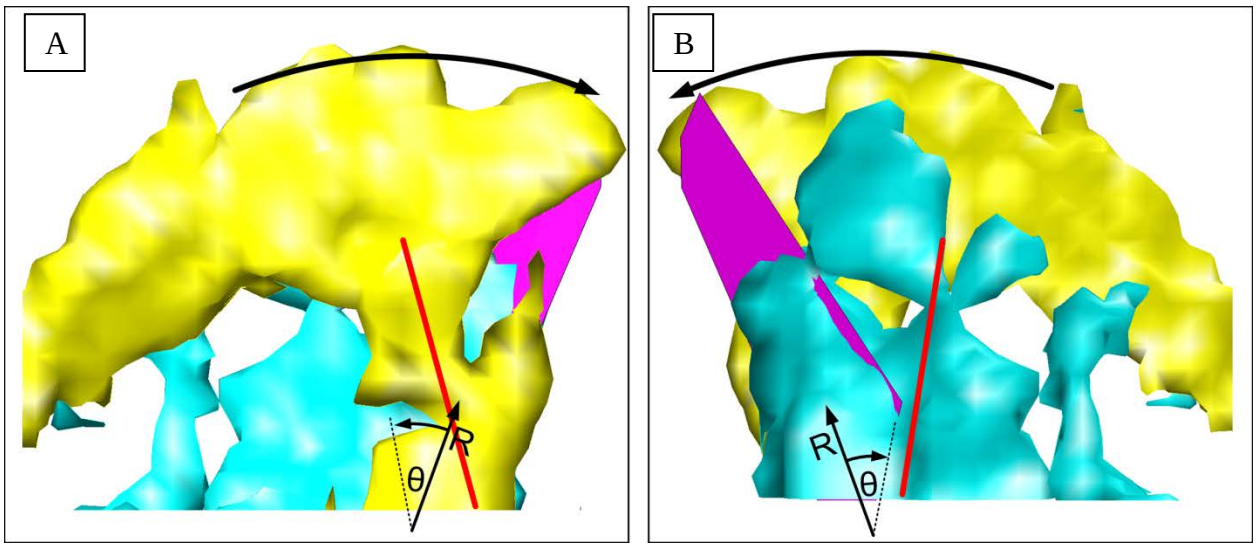

Figure 21: Elliptical Wing. (A) shows chordwise vorticity from the top of the wing and (B) shows chordwise vorticity from bottom of the wing. Yellow isosurface is ω= -2.5 1/s and cyan isosurface is ω = 1.5 1/s. Dark black line at wing tip shows direction of wing rotation. Red line shows general path of TEV.

Figure 20 (A) shows that there is a large distribution of chordwise vorticity from base to tip for both senses of chordwise vorticity with large concentrations near the tip. The concentration near the tip is due to the tip vortex having a mostly chordwise component of vorticity. It can also be seen that the chordwise vorticity increases from base to tip. In the region from the base to mid-span the chordwise vorticity is not from the tip vortex, so some of it must come from the tilting of the LEV and TEV. This can be seen along the red line where a nominal region of chordwise vorticity can be found.

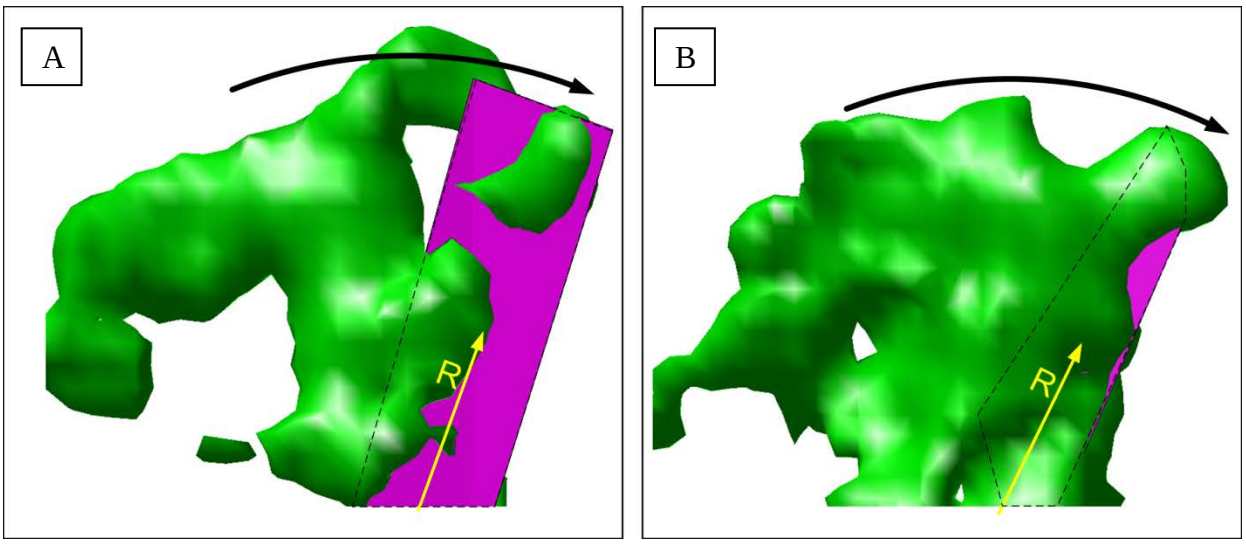

Figure 22: Spanwise flow for rectangular (A) and elliptical (B) wing shape. The isosurface value is ν = 1.5 cm/s for both cases (base to tip velocity). Dark black arrow represents direction of wing rotation.

For the spanwise flow, a similar approach is taken for visualization with an isosurface used to show the distribution. Figure 22 shows the spanwise flow in the radial direction. For the rectangular wing most of the spanwise flow is contained within the wake of the wing with a very distinct region of spanwise flow that coincides with the path of the tip vortex. This distinct path of spanwise flow is from the induced flow from the chordwise vorticity of the strong tip vortex.

In contrast for the elliptical wing Figure 22 (B), due to the weaker tip vortex the spanwise flow is more evenly dispersed.

4.3 CORRELATION OF VORTEX TILTING AND SPANWISE FLOW

The objective of this study is to show the correlation between the chordwise vorticity from the vortex tilting and the spanwise flow. To do this the chordwise vorticity was plotted on the same figure as the spanwise flow. From Figure 23 it can be seen that the spanwise flow occurs in a region that is between the positive (cyan) and negative (yellow) chordwise vorticity. The concentrated region of negative chordwise vorticity found near the tip is seen to induce a strong spanwise flow beneath it. Additionally, the chordwise vorticity from the vortex tiling between the base and mid-span of the wing is seen to induce a spanwise flow beneath it.

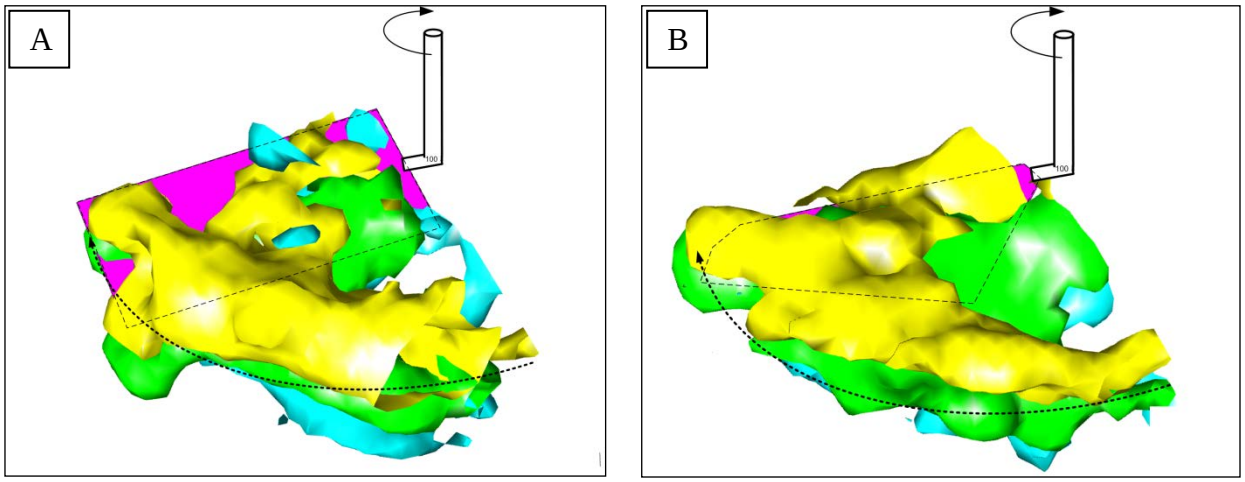

Figure 23: (A) is for rectangular case. Yellow ω = - 1.75 1/s and Cyan ω = 1.3 1/s. (B) is for elliptical case. Yellow ω= -2.5 1/s and cyan ω = 1.5 1/s. Both spanwise flows are ν = 1.5 cm/s.

Because the isosurfaces only show the distribution of vorticity and not variation in magnitude planar slices are taken at a position 25° downstream of the leading edge (refer to section 3.3). This planar slice gives a good indication of the chordwise vorticity and the spanwise

flow in the wake region of the wing. Figure 24 shows these planar slices for each wing shape and allow for a clear comparison between the regions of chordwise vorticity and the regions of spanwise flow.

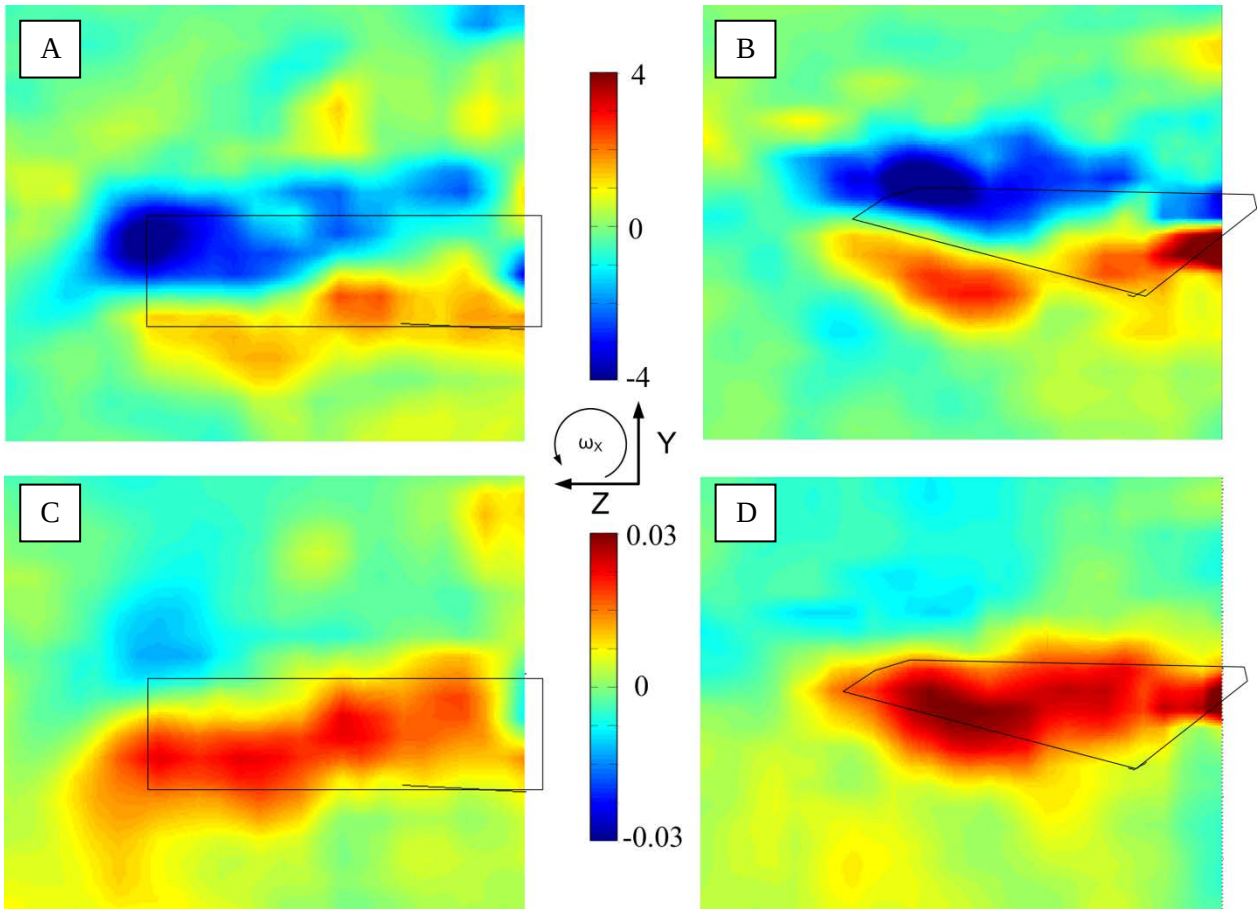

Figure 24: (A) and (B) show chordwise vorticity for the rectangular and elliptical wing respectively. Blue represents chordwise vorticity of LEV and red represents chordwise vorticity of TEV. Units of vorticity are 1/s. (C) and (D) represent spanwise velocity from base to tip (right to left) for the rectangular and elliptical wing respectively. Units of spanwise flow are m/s.

The rectangular wing shows a clear increase in negative (blue) chordwise vorticity from base to tip, with the darkest and strongest region at the tip. The positive (red) chordwise vorticity does not exhibit this same trend and reaches a maximum about 40% span and then steadily decreases. When comparing the chordwise vorticity in Figure 24 (A) with the spanwise flow in

Figure 24 (C) it is immediately obvious that the spanwise flow seems to follow a path in the region between the positive and negative chordwise vorticity. If we assume that vortex tilting is responsible for turning some of the spanwise vorticity of the LEV and TEV into chordwise vorticity in the region between the base and mid-span, then this observation supports the hypothesis that the chordwise vorticity that results from vortex tilting could enhance the spanwise flow.

4.4 RECTANGULAR WING VS. ELLIPTICAL WING

The rectangular wing provides a good benchmark for flow structures in flapping wing flight and a good comparison to Kim and Gharib [5]. Still, to make this study more relevant to insect flight, the elliptical wing that is modeled on the fruit fly will be analyzed and compared to the rectangular wing.

Figure 17 and Figure 18 show a clear difference in the tip vortex for each wing shape. The rectangular wing clearly has a stronger tip vortex as to be expected because of the tip condition. This can be seen by the more prominent flow structure coming off the tip of the rectangular wing. For the elliptical wing the tip vortex is not as prominent. Additionally the tip vortex for the elliptical wing seems to follow a path that is further from the path swept out by the tip. This may be explained by the earlier detachment of the LEV for the elliptical case as can be seen from Figure 25. From this figure, the LEV looks to detach at about 80-90% span on the rectangular wing as opposed to 60-70% span for the elliptical wing.

Figure 24 can be used to compare the chordwise vorticity of the rectangular wing to that of the elliptical wing. Here the negative chordwise vorticity for the elliptical wing is at a maximum at about 70% span, representing the core of the tip vortex. In contrast for the rectangular wing the maximum negative chordwise vorticity occurs at the wing tip (100% span)

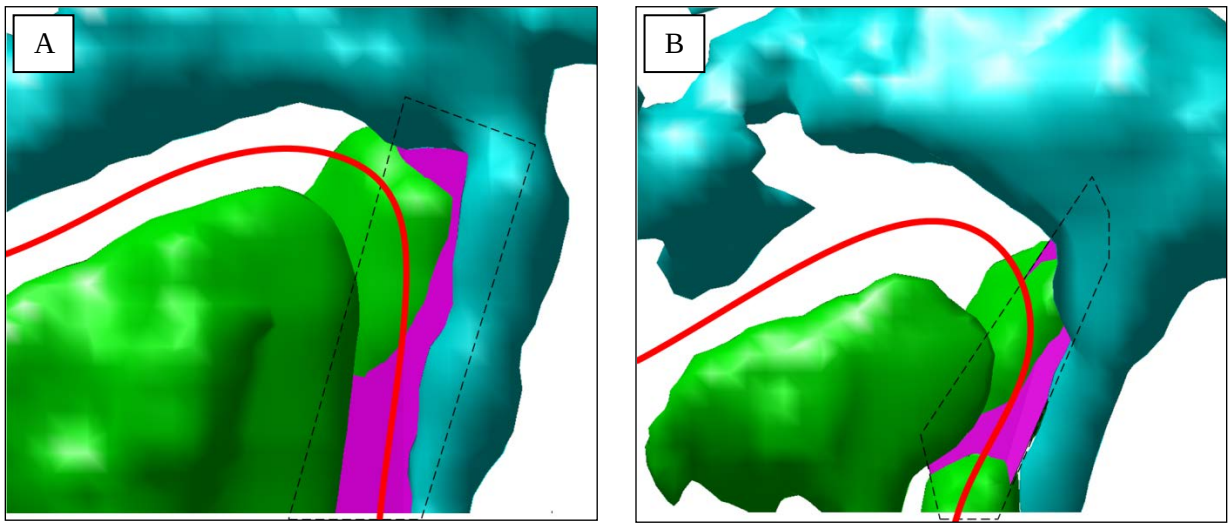

Figure 25: (A) Rectangular Wing shows upwash (cyan) and downwash (green) isosurfaces to visualize the path of the LEV. The red line represents the estimated center of the LEV. (B) Elliptical Wing.

from the strong tip vortex. This is an important feature because it shows that the LEV detaches and merges with the tip vortex at a shorter span location on the elliptical wing. Figure 25 also shows this earlier detachment, where the core of the LEV is represented by the red line. The LEV may detach from the elliptical wing earlier because the chord length decreases as span increases and eventually the chord length is too small to handle the large LEV as explained by Lentink and Dickinson [20].

Figure 24 also indicates that the regions of maximum spanwise flow seem to coincide with the regions of maximum chordwise vorticity for both wing shapes. For the rectangular case however, the spanwise flow continues all the way to the wing tip, likely because it is induced by the strong tip vortex present at the wing tip. For the elliptical case, the spanwise flow sharply drops off at about 80% of span after it has passed the region of strong chordwise vorticity from the tip vortex. This observation shows that the chordwise vorticity induced from the vortex tilting serves to induce a spanwise flow for both wing shapes.

If we once again assume that the chordwise vorticity induced by vortex tilting happens in the region between the wing base and mid-span, which is a reasonable assumption because the tip vortex is far from this region, then when inspecting Figure 24 it is apparent that there is both strong chordwise vorticity and strong spanwise flow in this region. This observation supports our hypothesis that chordwise vorticity induced by the vortex tilting of the LEV and TEV can indeed act to enhance the spanwise flow.

CHAPTER 5: SINUSOIDAL ANGULAR VELOCITY TEST CASE

The goal of analyzing the sinusoidal case is to study the development of the chordwise vorticity and spanwise flow as the velocity of the wing increases. In doing this, a more complete picture of the vortex dynamics can be attained to complete and complement the results from the constant velocity case. Many of the same visualization techniques employed in Chapter 4 will be used here.

For the purposes of this analysis, the frames 3, 4, 5, and 6 were chosen because they most clearly show the evolution of the spanwise flow and chordwise vorticity as the velocity increases from 50 mm/s to 90 mm/s tip velocity.

The tri-color isosurface in this case would not clearly show the evolution of the flow because of the acceleration of the wing. Instead, for this test case only, the chordwise vorticity and spanwise flow were plotted as in Section 4.1.3 for each frame. This will be shown in the next section.

Because of the advantage of plotting two dimensional slices for visualization of the wake, this method was also incorporated for this test case to more clearly show the correlation of the chordwise vorticity to the spanwise flow. This will be shown in section 5.2 and 5.3.

5.1 ISOSURFACES – CHORDWISE VORTICITY AND SPANWISE FLOW

To more clearly visualize the three-dimensional flow structures and the effects of vortex tilting on spanwise flow isosurfaces of chordwise vorticity and spanwise flow have been plotted for four different frames for each wing shape in Figure 26.

The negative chordwise vorticity is shown in yellow and is generated by the tilting of the LEV and the tip vortex. This can be seen for both cases, as the velocity increases the chordwise

vorticity becomes greater. Frame 1 has the least amount of chordwise vorticity, and as the wing accelerates, the isosurfaces of LEV and TEV chordwise vorticity grow due to the vortex tilting associated with the increasing velocity gradient from base to tip. It can also be seen, that as the chordwise vorticity increases, the spanwise flow, represented by the green isosurface, also increases. This is evidence that the spanwise flow is induced by the chordwise vorticity and increases as the chordwise vorticity increases for both the rectangular and elliptical wing.

For both wings, the large columnar shaped tip vortex is present downstream of the wing tip. However, the tip vortex for the rectangular wing is of much larger strength due to the induced drag from the sharp end. This makes sense because, as seen in aircraft, if a wing is tapered or rounded at the end (as with the elliptical wing) the induced drag associated with the strength of the tip vortex decreases [42].

The tip vortex can have a large effect on the spanwise flow near the tip of the wing and is seen to induce a large amount of spanwise flow beneath it in the wake area of the wing tip. In Frame 4 of the rectangular wing, this effect is especially present as the spanwise flow isosurface can be seen to extend very far into the wake. This is because in frame 4, the velocity of the wing tip is at a maximum, creating a relatively high strength tip vortex. This effect is not as visible for the elliptical wing because its tip vortex has a much lower strength in comparison to the tip vortex of the rectangular wing.

The increase in chordwise vorticity for the elliptical wing is very obvious when looking at the progression from frames one to four. In the first frame, there is almost no chordwise vorticity at all besides that at the wing tip. As the wing accelerates, the chordwise vorticity of the LEV immediately becomes visible in frame two and continues to increase all the way up to

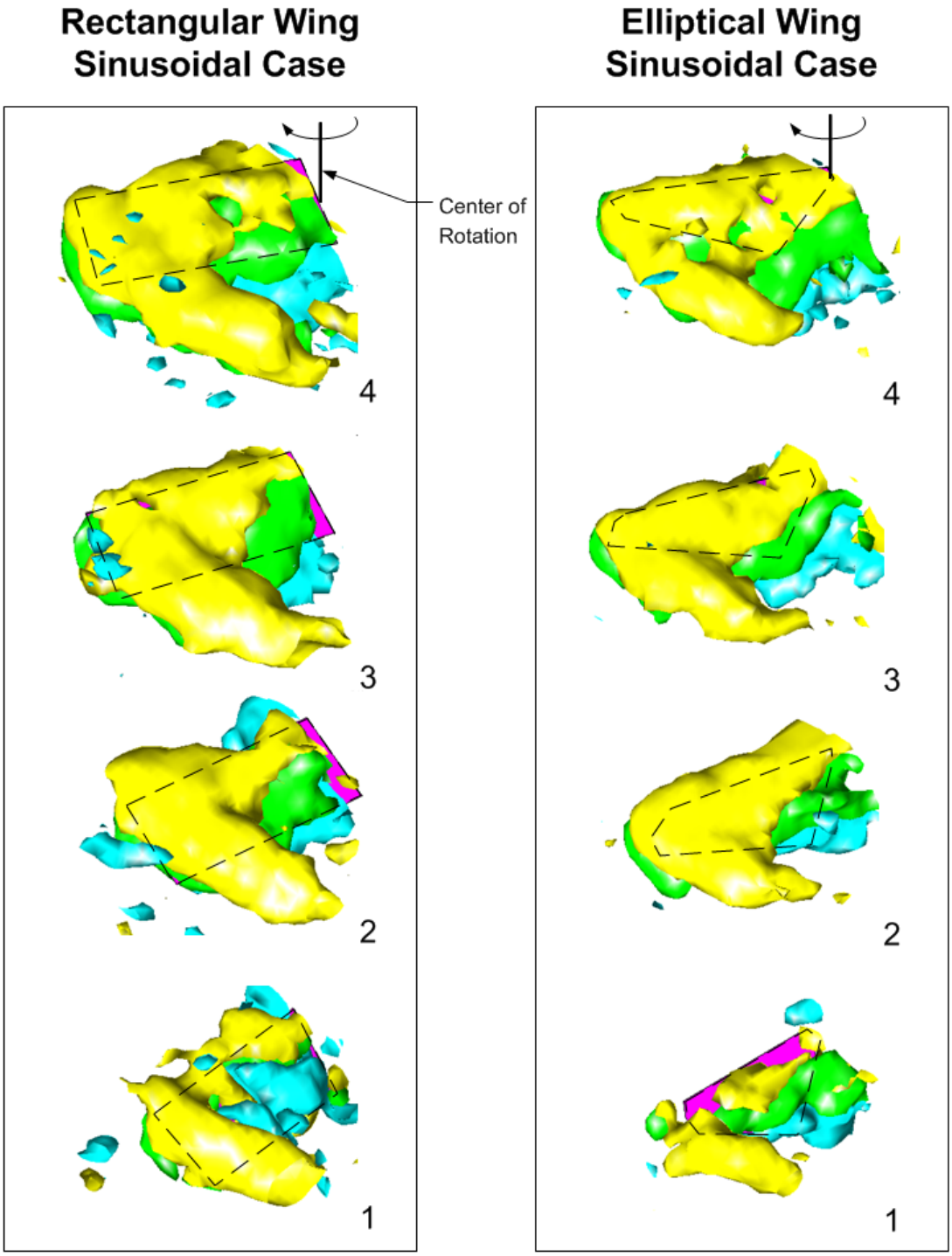

Figure 26: Isosurface plots for each different shaped wing as it rotates with the sinusoidal kinematic. Frames are 3, 4, 5 and 6 from the 10 frames captured, corresponding to 1,2,3 and 4 respectively in this figure. Yellow is negative chordwise vorticity from the LEV. Cyan is positive chordwise vorticity from the TEV. Green is spanwise flow from base to tip (right to left). Dotted line shows outline of wing. Note that some of wing may be out of the probe volume so the base of the wing may be cut off in frame one. Yellow is ω = - 1.75 1/s, Cyan ω = 1.3 1/s, Green is ν = 1.5 cm/s (base to tip) for all frames.

frame four. The spanwise flow follows the same trend as it increases from frame one to frame four. Because the vortex tilting increases the amount of chordwise vorticity, it thus increases the spanwise flow.

5.2 PLANAR SLICES – RECTANGULAR WING

To more clearly visualize the chordwise vorticity induced from the vortex tilting and its relation to the spanwise flow, planar slices were taken. These planar slices are approximately 6 mm downstream in the wake of the wing. This choice of position gave a good indication of the vortex dynamics downstream the wing in the region of the wake with the most intense spanwise flow. The advantage of these slices is that the varying magnitude of chordwise vorticity and spanwise flow could easily be viewed.

For the rectangular case (Figure 27) the first frame plotting the chordwise vorticity clearly shows the negative vorticity associated with the tip vortex. The correlating frame with spanwise flow (frame to the right) shows the beginning stages of the induced spanwise flow from the tip vortex. This can be seen by the small region of red and orange in the region below the tip vortex in frame 1. In this same frame there are also the beginning stages of the spanwise flow being generated near the base of the wing and another region near the tip. It is interesting to note that each of these regions of spanwise flow have not yet merged, indicating that it is being induced by different means, one region by the tip vortex and the other by the TEV.

As the wing accelerates the tip vortex grows much stronger, indicated by the dense region of blue for the chordwise vorticity frames two, three, and four. Additionally, from frames two to four the LEV tilting becomes more prominent, which can be seen by the increasing chordwise vorticity at the top of the wing (blue region). Also the TEV's strength is increasing, with it spanning nearly the entire wing by the third frame (red region at bottom of the wing).

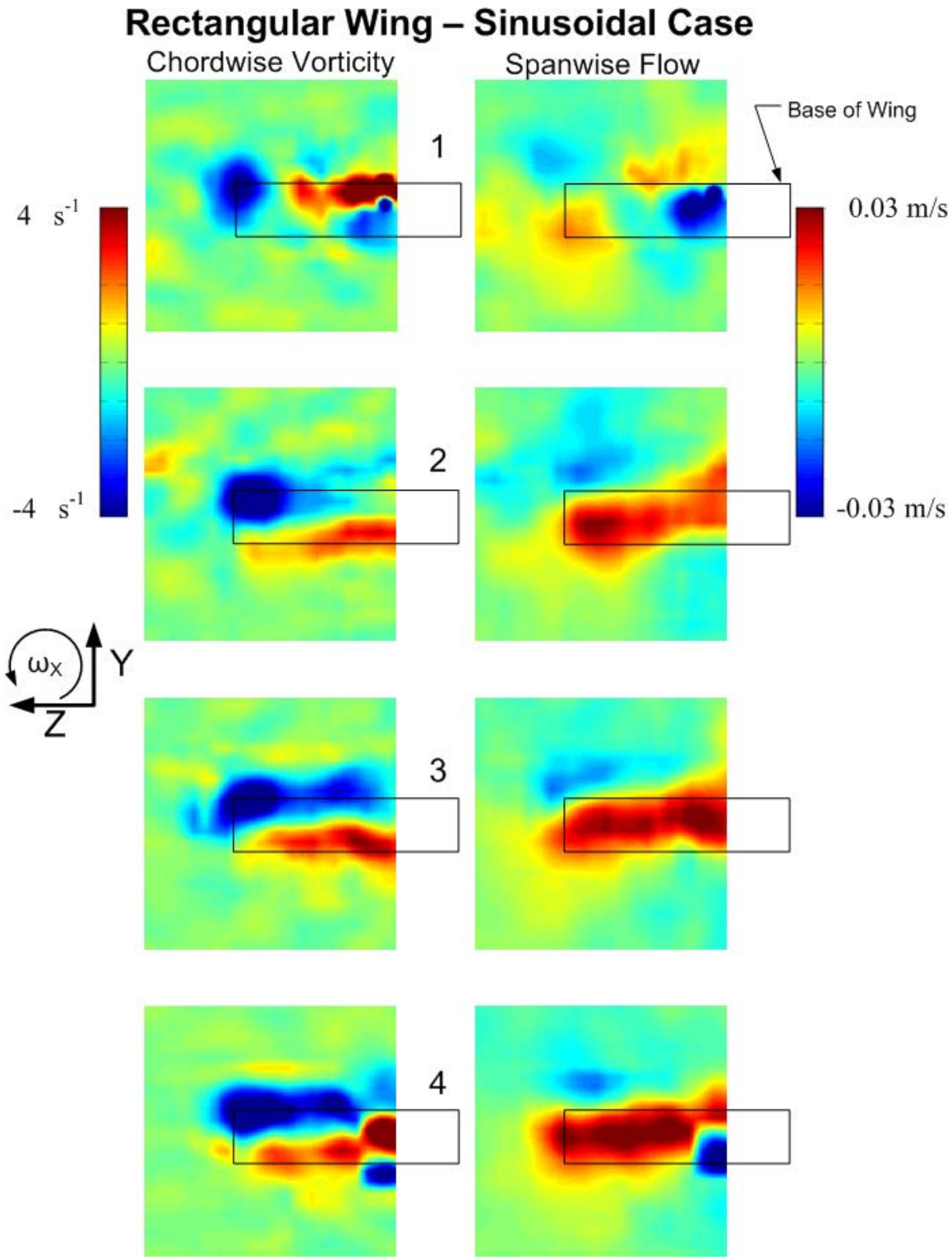

Figure 27: Planar slices for rectangular wing. (Left) Chordwise vorticity. Blue represents clockwise rotation and red represents counterclockwise rotation. (Right) Spanwise flow (positive from right to left). Frames go in chronological order from 1 to 4. Chordwise vorticity frame on right corresponds with spanwise flow frame on left. Movement of the wing is into the page. Looking from back of wing.

With the increasing chordwise vorticity of the LEV and TEV comes an increase in spanwise flow, represented by the dense regions of red in the spanwise flow planes from frames two to four.

From these images, the correlation between the position of the spanwise flow and the chordwise vorticity can be clearly seen. The region of small vorticity between the positive and negative chordwise vorticity (blue and red) is coincident with the region of spanwise flow. This simple position correlation supports that the spanwise flow is indeed being induced by the chordwise vorticity of the LEV, TEV, and tip vortex.

It is also interesting that the most concentrated region of spanwise flow does not occur at the tip of the wing but a region near the mid-span of the wing. When viewing the corresponding chordwise vorticity plots, the location of the concentrated spanwise flow coincides with the regions where the chordwise vorticity of the LEV and TEV are close in position and strength (near the middle of the wing).

5.3 PLANAR SLICES – ELLIPTICAL WING

For the elliptical wing, the same planar slices were taken as for the rectangular wing. Figure 28 shows these slices. It is immediately obvious that there is a tip vortex that is present near the tip of the wing, indicated by the light blue region. However this tip vortex is not all the way at the tip of the wing, and rather it is at about 85% span. This could be due to the LEV shedding near about 75% span for the elliptical wing.

The LEV for the elliptical wing clearly begins to tilt starting at the wing tip and moves toward the base as the wing accelerates. This can be seen from frames two to four. In frame two the region of blue (chordwise vorticity of the LEV) only extends slightly from the wing tip. As the wing accelerates and the vortex tilting becomes more prominent, the chordwise vorticity

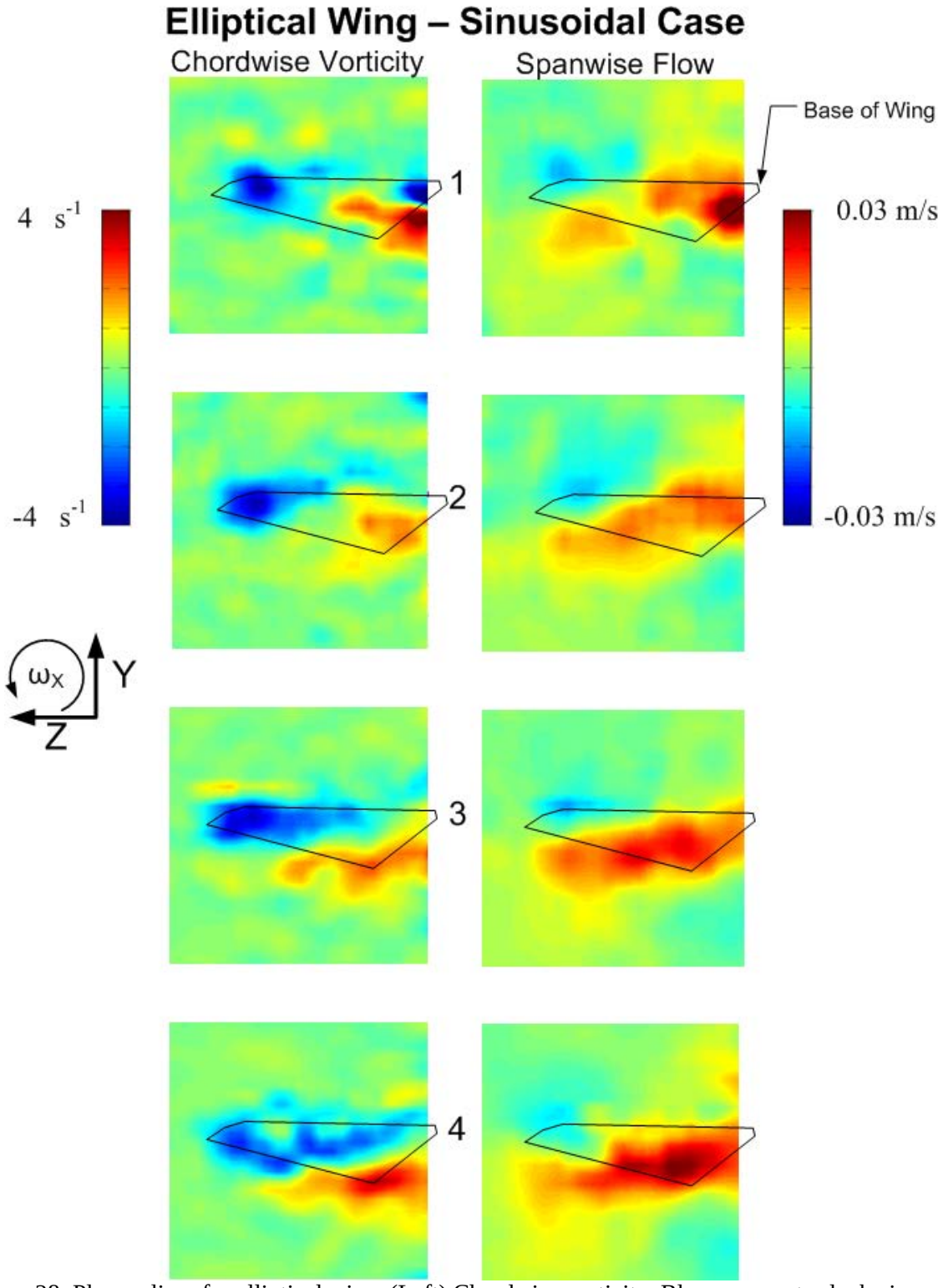

Figure 28: Planar slices for elliptical wing. (Left) Chordwise vorticity. Blue represents clockwise rotation and red represents counterclockwise rotation. (Right) Spanwise flow (positive from right to left). Frames go in chronological order from 1 to 4. Chordwise vorticity frame on right corresponds with spanwise flow frame on left. Velocity of the wing is into the page. Looking at it from back of wing.

moves closer and closer to the wing base. This can be seen in frame three, as the region on blue now extends from the tip to about 30% span. By frame four, the chordwise vorticity of the LEV has fully extended all the way from the tip to the base.

The chordwise vorticity of the TEV begins at the base (instead of the tip as the in the LEV) and increases toward the tip as the wing accelerates. This evolution can be seen from frames one to four. In the first and second frame, the chordwise vorticity of the TEV is mostly confined to a region from 0% to about 30% span. As the wing accelerates and the vortex tilting becomes more prominent, the chordwise vorticity of the TEV begins to move toward the tip until it reaches roughly 75% span in frame four. It is interesting that the LEV tilting and the TEV tilting evolve in opposite directions, but expected, because the different rotational signs of each.

For the spanwise flow the trend is the same as in all the previous cases. As the chordwise vorticity of the LEV and TEV become stronger the spanwise flow increases. In the first frame there are two distinct regions of spanwise flow, one near the tip, induced by the tip vortex, and on near the base, induced by the chordwise vorticity of the TEV. From frames two to four the spanwise flow increases as the chordwise vorticity increases, following the same trend as the rectangular wing. Additionally, as in the rectangular wing case, the most concentrated region of spanwise flow occurs near the middle of the wing span. This is believed to be due to the strength and proximity of the chordwise vorticity of the LEV and TEV, which can be seen in frame four.

5.4 RECTANGULAR WING VS. ELLIPTICAL WING

The main differences between the rectangular and elliptical wing for the sinusoidal kinematic case lie in the strength and location of the chordwise vorticity and spanwise flow.

First the tip vortex of the rectangular wing is much stronger than the elliptical wing, and also, it is located at 100% span, as opposed to 85% span for the elliptical wing. This is to be

expected because the rounding and tapering of the elliptical wing decreases the strength of the tip vortex. This can be further quantified by the higher Oswald Efficiency Factor of the elliptical wing (≈1.0) as opposed to the Oswald efficiency factor of about 0.8 for a rectangular wing [43].

The magnitude of the LEV and TEV tilting is also much larger for the rectangular wing. This can be seen when looking at Figure 27, as the colors are much darker than the elliptical wing in Figure 28. This is because of the larger wing area of the rectangular wing. The higher strength of the LEV and TEV for the rectangular wing is also tied to its higher magnitude of spanwise flow.

The spanwise flow for the rectangular wing is much higher in magnitude than the spanwise flow of the elliptical wing. This is due to the higher strength of the chordwise vorticity of the LEV and TEV, as stated above.

As far as the overall distribution of the chordwise vorticity and the spanwise flow, the rectangular wing and elliptical wing are very similar. The spanwise flow for both wings exhibit a trend toward the bottom of the wing as span percentage increases (from base to tip).

The consistency of the overall location of the prominent features of each wing indicates that the shape of the wing does not greatly affect the overall distribution of the LEV, TEV, and spanwise flow.

CHAPTER 6: CONCLUSIONS AND FUTURE WORK

6.1 SUMMARY OF RESULTS

A novel 3D PIV system was utilized to study the flow structures of a rectangular and elliptical wing undergoing constant rotation and sinusoidal rotation. The 3D ability of the V3V system allowed for the study of vortex tilting, which is absent in 2D flows.

Both the chordwise vorticity and the spanwise flow were visualized using isosurfaces and planar slices. The isosurfaces for every test case and wing shape showed that the spanwise flow occurred in a region that was between the positive and negative chordwise vorticity. The planar slices supported this observation and also indicated that the magnitude of the spanwise flow was related to the position and strength of the chordwise vorticity. The location of the highest spanwise flow coincided with the region of the highest concentration of the positive and negative chordwise vorticity, which occurred near the mid-span of each wing.

The detachment of the LEV was seen to occur at a larger span percentage for the rectangular wing (80%) than the elliptical wing (60%). This is due to the smaller chord length near the wing tip for the elliptical wing and is consistent with other findings. This is consistent with the findings that the spanwise flow extended closer to the tip for the rectangular wing than the elliptical wing, as seen in the planar slices.

The sinusoidal kinematic test case showed more information in regards to the evolution of the flow than the constant velocity test case. From the sinusoidal case it was observed that there are two distinct regions of spanwise flow that develop at the beginning stages of the wing stroke. As the wing accelerates, the two regions of spanwise flow unionize and become one. The spanwise flow for each wing takes a path starting at the top of the wing near the base and ending at the bottom of the wing near the tip, so it is diagonal.

Additionally it was observed that the general distribution of vorticity around the different wing shapes was nearly the same. This indicates that different wing shapes do not greatly affect the distribution of vorticity about the wing.

6.2 HYPOTHESIS VERIFICATION

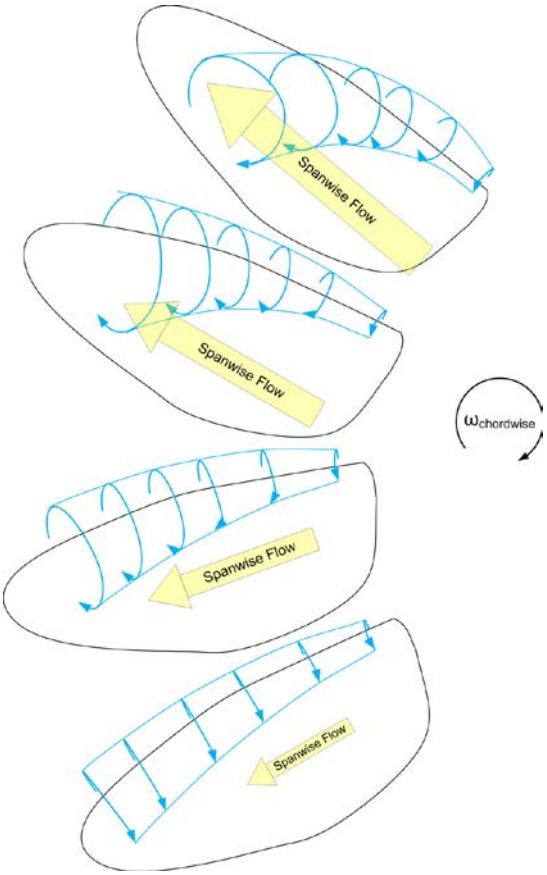

Figure 29: Hypothesis of vortex tilting inducing spanwise flow. The velocity of the wing is increasing from the bottom frame to the top frame as is the tilting of the LEV. The TEV is not shown here but has a similar effect.

With a rotating wing, as the angular velocity increases the tangent velocity also increases from base to tip. Based on theory, vortex tilting increases as the velocity gradient increases. It then follows that the vortex tilting of the LEV and TEV would increase, and thus the chordwise vorticity will increase as the wing velocity increases. It was observed that as the chordwise vorticity increased the spanwise flow increased. This occurred in a region between the LEV and

TEV, thus it was found that there is a strong correlation between the vortex tilting and spanwise flow.

Figure 29 shows a schematic of the hypothesis. Observe that as the velocity increases the tilting of the LEV also increases (TEV not shown here). With this increase in chordwise vorticity the spanwise flow increased as well.

6.3 FUTURE WORK

In the future, a more complete theoretical study involving vortex tilting needs to be carried out to further explain the evolution of vortex tilting in flapping wing flight. Additionally, more work needs to be done to investigate the effect of vortex stretching on LEV attachment [44].

To supplement the findings in this study, more experimental work needs to be carried out using more complex wing kinematics that are representative of realistic wing motions in insect flight that incorporate wing-wing and wing-wake interaction. Higher Reynolds numbers such as those of a Hawkmoth (Re=4000) also need to be experimentally tested using V3V to obtain a better picture of the difference in flow structure from the low Reynolds number data obtained here.

Quantitatively there is much that still needs to be done. The calculation of circulation, vortex tilting, and vortex stretching is the next step. These numbers can serve to validate the qualitative work presented here.

Additionally, with quantitative spanwise flow information, the amount of vorticity drained into the wake could be estimated and balanced with the amount of vorticity generated at the leading edge. If the amount of vorticity drained is comparable with the vorticity generated,

then this calculation could be a robust test of the hypothesis that spanwise flow is the primary stabilizer of the LEV in flapping wing flight.

LIST OF REFERENCES

[1] Polhamus, E. C., 1971, "Predictions of Vortex-Lift Characteristics by a Leading-Edge Suction Analogy," Journal of Aircraft, Volume 8(Number 4), p. 193.

[2] Birch, J. M., and Dickinson, M. H., 2001, "Spanwise flow and the attachment of the leading-edge vortex on insect wings," Nature, 412(6848), pp. 729-733.

[3] Ellington, C. P., vandenBerg, C., Willmott, A. P., and Thomas, A. L. R., 1996, "Leading-edge vortices in insect flight," Nature, 384(6610), pp. 626-630.

[4] TSI, I., "V3V - Recent Applications," Proc. American Physics Society Division of Fluid Dynamics, pp. 1-54.

[5] Kim, D., and Gharib, M., 2010, "Experimental study of three-dimensional vortex structures in translating and rotating plates," Experiments in Fluids, 49(1), pp. 329-339.

[6] Flammang, B. E., Lauder, G. V., Troolin, D. R., and Strand, T. E., 2011, "Volumetric imaging of fish locomotion," Biology Letters, 7(5), pp. 695-698.

[7] Sane, S. P., 2003, "The aerodynamics of insect flight," Journal of Experimental Biology, 206(23), pp. 4191-4208.

[8] Anderson, J. D., 1991, Fundamentals of aerodynamics / John D. Anderson, Jr, McGraw-Hill, New York.

[9] Dickinson, M. H., Lehmann, F. O., and Sane, S. P., 1999, "Wing rotation and the aerodynamic basis of insect flight," Science, 284(5422), pp. 1954-1960.

[10] Maxworthy, T., 1979, "EXPERIMENTS ON THE WEIS-FOGH MECHANISM OF LIFT GENERATION BY INSECTS IN HOVERING FLIGHT .1. DYNAMICS OF THE FLING," Journal of Fluid Mechanics, 93(JUL), pp. 47-&.

[11] Dickinson, M. H., and Gotz, K. G., 1993, "UNSTEADY AERODYNAMIC PERFORMANCE OF MODEL WINGS AT LOW REYNOLDS NUMBERS," Journal of Experimental Biology, 174(1), pp. 45-64.

[12] Lehmann, F. O., 2004, "The mechanisms of lift enhancement in insect flight," Naturwissenschaften, 91(3), pp. 101-122.

[13] Maxworthy, T., 1981, "THE FLUID-DYNAMICS OF INSECT FLIGHT," Annual Review of Fluid Mechanics, 13, pp. 329-350.

[14] Shyy, W., and Lin, H., 2007, "Flapping wings and aerodynamic lift: The role of leading-edge vortices," Aiaa Journal, 45(12), pp. 2817-2819.

[15] Kundu, P. K., and Cohen, I. M., 2004, Fluid Mechanics, Elsevier Academic Press, San Diego, CA.

[16] Minotti, F. O., and Speranza, E., 2005, "Leading-edge vortex stability in insect wings," Physical Review E, 71(5), p. 051908.

[17] Lentink, D., and Dickinson, M. H., 2009, "Rotational accelerations stabilize leading edge vortices on revolving fly wings," Journal of Experimental Biology, 212(16), pp. 2705-2719.

[18] Birch, J. M., Dickson, W. B., and Dickinson, M. H., 2004, "Force production and flow structure of the leading edge vortex on flapping wings at high and low Reynolds numbers," Journal of Experimental Biology, 207(7), pp. 1063-1072.

[19] Shyy, W., Trizila, P., Kang, C. K., and Aono, H., 2009, "Can Tip Vortices Enhance Lift of a Flapping Wing?," Aiaa Journal, 47(2), pp. 289-293.

[20] Lentink, D., and Dickinson, M. H., 2009, "Biofluiddynamic scaling of flapping, spinning and translating fins and wings," Journal of Experimental Biology, 212(16), pp. 2691-2704.

[21] Ringuettet, M. J., Milano, M., and Gharib, M., 2007, "Role of the tip vortex in the force generation of low-aspect-ratio normal flat plates," Journal of Fluid Mechanics, 581, pp. 453-468.

[22] Trizila, P., Kang, C.-K., Aono, H., Visbal, M., and Shyy, W., 2010, "Fluid Physics and Surrogate Modeling of a Low Reynolds Number Flapping Rigid Flat Plate " 28th AIAA Applied Aerodynamics Conference, AIAA, Chicago, Illinois.

[23] Sane, S. P., 2006, "Induced airflow in flying insects - I. A theoretical model of the induced flow," Journal of Experimental Biology, 209(1), pp. 32-42.

[24] Sane, S. P., and Jacobson, N. P., 2006, "Induced airflow in flying insects - II. Measurement of induced flow," Journal of Experimental Biology, 209(1), pp. 43-56.

[25] Kim, D., and Gharib, M., 2010, "Visualization of three-dimensional vortex dynamics and fluid transport in translating plates, using defocusing DPIV.," 15th

International Symposium on Applications of Laser Techniques to Fluid MechanicsLisbon, Portugal.

[26] Troolin, D. R., and Longmire, E. K., 2010, "Volumetric velocity measurements of vortex rings from inclined exits," Experiments in Fluids, 48(3), pp. 409-420.

[27] TSI, I., "V3V - Recent Appications," Proc. American Physics Society Division of Fluid Dynamics, pp. 1-54.

[28] Suryadi, A., Ishii, T., and Obi, S., 2010, "Stereo PIV measurement of a finite, flapping rigid plate in hovering condition," Experiments in Fluids, 49(2), pp. 447-460.

[29] Lu, Y., and Shen, G. X., 2008, "Three-dimensional flow structures and evolution of the leading-edge vortices on a flapping wing," Journal of Experimental Biology, 211(8), pp. 1221-1230.

[30] Poelma, C., Dickson, W. B., and Dickinson, M. H., 2006, "Time-resolved reconstruction of the full velocity field around a dynamically-scaled flapping wing," Experiments in Fluids, 41(2), pp. 213-225.

[31] Babinsky, H., and Jones, A. R., "Unsteady Lift Generation on Sliding and Rotating Flat Plate Wings," Proc. AIAA Fluid Dynamics Conference, AIAA, ed., AIAA.

[32] Combes, S. A., and Daniel, T. L., 2001, "Shape, flapping and flexion: Wing and fin design for forward flight," Journal of Experimental Biology, 204(12), pp. 2073-2085.

[33] Taira, K., and Colonius, T., 2009, "Three-dimensional flows around low-aspect-ratio flat-plate wings at low Reynolds numbers," Journal of Fluid Mechanics, 623, pp. 187-207.

[34] Taira, K., Dickson, W. B., Colonius, T., Dickinson, M. H., and Rowley, C. W., "Unsteadiness in flow over a flat plate at angle-of-attack at low Reynolds numbers," Proc. 45th AIAA Aerospace Sciences Meeting and Exhibit, AIAA, ed., AIAA.

[35] Ozen, C. A., and Rockwell, D., 2011, "Vortical structures on a flapping wing," Experiments in Fluids, 50(1), pp. 23-34.

[36] Jones, A. R., and Babinsky, H., 2011, "Reynolds number effects on leading edge vortex development on a waving wing," Experiments in Fluids, 51(1), pp. 197-210.

[37] Kweon, J., and Choi, H., 2010, "Sectional lift coefficient of a flapping wing in hovering motion," Physics of Fluids, 22(7), p. 4.

[38] Sane, S. P., and Dickinson, M. H., 2002, "The aerodynamic effects of wing rotation and a revised quasi-steady model of flapping flight," Journal of Experimental Biology, 205(8), pp. 1087-1096.

[39] Sane, S. P., and Dickinson, M. H., 2001, "The control of flight force by a flapping wing: lift and drag production," Journal of Experimental Biology, 204(15), pp. 2607-2626.

[40] Shyy, W., Aono, H., Chimakurthi, S. K., Trizila, P., Kang, C. K., Cesnik, C. E. S., and Liu, H., 2010, "Recent progress in flapping wing aerodynamics and aeroelasticity," Progress in Aerospace Sciences, 46(7), pp. 284-327.

[41] Zhao, L., Huang, Q., Deng, X., and Sane, S. P., 2010, "Aerodynamic effects of flexibility in flapping wings," J R Soc Interface, pp. 485-497.

[42] Anderson, J. D., 2005, Introduction to flight / John D. Anderson, Jr, McGraw-Hill Higher Education, Boston.

[43] Raymer, D. P., 1999, Aircraft design : a conceptual approach / Daniel P. Raymer, American Institute of Aeronautics and Astronautics, Reston, VA.

[44] Lim, T. T., Teo, C. J., Lua, K. B., and Yeo, K. S., 2009, "ON THE PROLONG ATTACHMENT OF LEADING EDGE VORTEX ON A FLAPPING WING," Modern Physics Letters B, 23(3), pp. 357-360.